AWARD NUMBER: W81XWH-17-1-0203

TITLE: Criticality of the phosphate carrier SLC25A3 for mitochondrial inorganic phosphate uptake to sustain striated muscle function

PRINCIPAL INVESTIGATOR: Dr. Erin Seifert

CONTRACTING ORGANIZATION: Thomas Jefferson University, Philadelphia, PA

REPORT DATE: January 2023

TYPE OF REPORT: Final

PREPARED FOR: U.S. Army Medical Research and Development Command
Fort Detrick, Maryland 21702-5012

REPORT DOCUMENTATION PAGE

Form Approved
OMB No. 0704-0188

PLEASE DO NOT RETURN YOUR FORM TO THE ABOVE ADDRESS.

1. REPORT DATE *(DD-MM-YYYY)*	2. REPORT TYPE	3. DATES COVERED *(From - To)*
January 2023	Final	30Sep2017 – 29Sep2022

4. TITLE AND SUBTITLE

Criticality of the phosphate carrier SLC25A3 for mitochondrial inorganic phosphate uptake to sustain striated muscle function

5a. CONTRACT NUMBER

W81XWH-17-1-0203

5b. GRANT NUMBER

5c. PROGRAM ELEMENT NUMBER

6. AUTHOR(S)

Erin Seifert
E-Mail: erin.seifert@jefferson.edu

5d. PROJECT NUMBER

5e. TASK NUMBER

5f. WORK UNIT NUMBER

7. PERFORMING ORGANIZATION NAME(S) AND ADDRESS(ES)

Thomas Jefferson University
833 Chestnut St., Suite 900
Philadelphia PA 19107-4418

8. PERFORMING ORGANIZATION REPORT NUMBER

9. SPONSORING/MONITORING AGENCY NAME(S) AND ADDRESS(ES)

U.S. Army Medical Research and Development Command
Fort Detrick, Maryland 21702-5012

10. SPONSOR/MONITOR'S ACRONYM(S)

11. SPONSOR/MONITOR'S REPORT NUMBER(S)

12. DISTRIBUTION/AVAILABILITY STATEMENT

Approved for Public Release; Distribution Unlimited

13. SUPPLEMENTARY NOTES

14. ABSTRACT

This project investigates the criticality of the mitochondrial phosphate carrier (PiC) for oxidative phosphorylation (oxphos; Aim 1) and buffering of mitochondrial matrix Ca2+ (Aim 2). Aim 3 focuses on the generation of TAT fusion proteins for the PiC and their ability to rescue phenotypes induced by PiC depletion. In this reporting period (Nov 2020 – Oct 2021), substantial progress was made on Aims 2 and 3. For Aim 2, we have almost completed a manuscript that investigates the role of the PiC in mitochondrial Ca2+ handling and the implications on cytosolic Ca2+ signaling in muscle fibers and force generation of intact muscle. These studies utilized a new mouse model in which PiC is deleted specifically in skeletal muscle (skm), in a Tamoxifen-inducible fashion. For the experiments, PiC was deleted by injecting 9-week old mice with Tamoxifen; skm mitochondria, intact fibers and whole muscle were harvested 2 weeks later at which point PiC protein was only ~5-10% of normal levels.

15. SUBJECT TERMS

Inorganic phosphate, Mitochondrial inner membrane transporters, Oxidative phosphorylation, Mitochondrial calcium uptake, TAT fusion protein, Mitochondrial myopathy, Mitochondrial disease, Nutrient signaling in skeletal muscle

16. SECURITY CLASSIFICATION OF:			17. LIMITATION OF ABSTRACT	18. NUMBER OF PAGES	19a. NAME OF RESPONSIBLE PERSON
a. REPORT	b. ABSTRACT	c. THIS PAGE			USAMRDC
Unclassified	Unclassified	Unclassified	Unclassified	70	19b. TELEPHONE NUMBER *(Include area code)*

Table of Contents

1. INTRODUCTION

This project investigates the criticality of the mitochondrial phosphate carrier (PiC) for the two main processes within mitochondria that require inorganic phosphate, namely oxidative phosphorylation (oxphos) and buffering mitochondrial matrix Ca^{2+}. Experiments were organized into 3 Aims. Aim 1 directly investigates the required of PiC for oxphos and also investigates adaptive mechanisms that counter loss of PiC which are important to consider in the context of natural pathogenic mutations in the human gene SLC25A3 encoding PiC; these mutations lead to myopathies. Aim 2 investigates the requirement of PiC for buffering mitochondrial Ca^{2+} as well as the downstream impact on cellular Ca^{2+} signaling; indeed, mitochondria can take up a vast amount of Ca^{2+} and, as such, participate in cellular Ca^{2+} homeostasis. Changes to how mitochondria handle Ca^{2+} are expected to have a broader effect on cell functions affected by Ca^{2+}. Aim 3 turns to the potential use of a TAT fusion protein as a therapeutic tool to manage myopathies resulting from mutations in human SLC25A3. The goal of Aim 3 is to generate TAT fusion proteins for both PiC isoforms (A and B), then to determine if the fusion proteins can rescue phenotypes caused by PiC depletion. Thus this project is expected to 1) advance our basic knowledge about a fundamental process, namely supplying inorganic phosphate to mitochondria for critical functions performed by mitochondria, and 2) to generate a potential therapeutic tool for a subset of human myopathies.

2. KEYWORDS

-Inorganic phosphate

-Mitochondrial inner membrane transporters

-Oxidative phosphorylation

-Mitochondrial calcium uptake

-TAT fusion protein

-Mitochondrial myopathy

-Mitochondrial disease

-Nutrient signaling in skeletal muscle

Section 3 – Accomplishments

Please find below the Specific Aims, the Major tasks, and sub-tasks, as these appear in the Statement of Work (SOW) that was part of the grant. Provided for each sub-task is a description of the result that was obtained, together with the Figure number that appears in the manuscript drafts that follow.

Statement of the Specific Aims

Aim 1: To evaluate if PiC is critically required to transport inorganic phosphate into the mitochondrial matrix, and mechanisms that counteract PiC deficiency.

Aim 2: To test if PiC deficiency causes dysregulation of cytoplasmic and mitochondrial Ca^{2+} and Ca^{2+} regulated functions.

Aim 3: To generate TAT fusions proteins of PiC and to test if TAT-PiC can be delivered to cells.

Major Tasks and sub-tasks

Major Task 1 - Part of Aim 1 (approval of vertebrate animal use, validation of the mouse model), Part of Aim 3 (TAT-PiC-A/B generation, purification, validation)

1) USAMRMC Animal Care and Use Review Office and Local IACUC Approval (Aim 1).

We obtained approval to use vertebrate animals (mouse model of skeletal muscle (SM)-specific depletion of the mitochondrial phosphate carrier (PiC)), both IACUC and ACURO. Subsequently, we bred the mice to obtain mice with SM-specific depletion of PiC (PiC KD mice, or "KD" for knockdown) and littermate control mice (SM-PiC-fl/fl – Control, or "Ctrl"). To confirm that the mouse was as expected, namely KD of PiC in SM only, we performed western blot analysis using a validated antibody against the PiC on tissues lysates of SM (Quadriceps, Soleus, Flexor digitorum brevis), heart, brain, kidney, and liver. As expected, based on the design of the mouse model, PiC was depleted only in SM. **See Part 1, Figure 1A, Part 1, Suppl Fig. 1**.

Sub-task was fully accomplished.

2) To design and construct both TAT-PiC-A and TAT-PiC-B isoforms. Choosing the bacterial host for the expression of the TAT-PiCA/B fusion proteins. (Aim 3)

Humans (and mice) have a documented alternatively spliced exon 3A and 3B, generating two PiC isoforms, A and B. Thus, we designed and constructed TAT-PiC-A and TAT-PiC-B *human* isoforms. To target both TAT proteins to the mitochondria, the natural mitochondrial targeting sequence (MTS) of PiC (49 aa) was included (**Part 2, Figure 1: schematic**).

The sequence encoding the chimeric protein was inserted into a pet28 expression vector under the control of the T7 promoter. A schematic of the final chimeric proteins, TAT-MTS-PiC-A and TAT-MTS-PiC-B, is shown in **Part 2, Figure 2A**. To confirm the coding sequence of both chimeric proteins, sequencing analysis was performed. **Part 2, Figure 2B** shows the full amino acid sequences of TAT-MTS-PiC-A and TAT-MTS-PiC-B fusion proteins.

To determine which bacterial system to use, we started with the TAT-MTS-PiCA fusion protein. The TAT chimeric protein was expressed in various bacterial expression systems, under different conditions (not shown). The most successful expression system proved to be the HMS strain of *E. coli* bacteria strain, grown at 37°C, after induction with 1mM IPTG for 2-3 hrs at 37°C (not shown).

Sub-task was fully accomplished.

3) Calibrating the conditions for high expression levels of the fusion proteins in a bacterial host (Aim 3).

After expressing the TAT chimeric protein in bacteria, different subcellular fractions were prepared: whole cell extract (WCE), soluble fraction (Sol) and inclusion bodies (IB). Each fraction was separated on a gel under denaturing conditions. To visualize all proteins on the gel, the gel was stained with Coomassie blue. Immunoblot analyses was performed using an anti-His tag antibody (to detect the His tags of the TAT construct) as well as human anti-PiC antibodies (Sigma). The Coomassie blue staining revealed bands with estimated masses corresponding to those of the

expressed TAT chimeric protein (~43kDa: **see Part 2, Figure 3**). Western blot analyses using antibodies specific to His (**Figure 3**) and human PiC (not shown) confirmed the identity of the fusion protein. Because PiC is a membrane protein, as expected, the subcellular fraction with the largest amount of TAT-MTS-PiC-A was the IB (not shown). These analyses confirm the successful expression of the in-frame, full-length fusion protein.
TAT-PiC-B was successfully generated according to the same procedures and, like TAT-PiC-A, found mostly to be in IB.
Sub-task was fully accomplished.
4) Purification of the TAT-PiC-A/B fusion proteins (Aim 3).
To purify TAT-PiC-A/B, bacteria were thawed and suspended in lysis buffer (20 mM Tris-HCl, pH 8.0; 0.05 M NaCl; 0.2 mg/ml lysozyme; 1 mM phenylsullfonyl fluoride (PMSF)) for 30 minutes at room temperature, then sonicated. A sample was taken from the lysed cells and marked as whole cell extract (WCE). The remaining sample was centrifuged at 17,500 g for 30 min. The supernatant (soluble fraction; sol) was removed and the pellet (containing inclusion bodies) was suspended in denaturation buffer, then cleared by centrifugation at 17,500 g for 30 min. The supernatant, containing denatured proteins, was collected and marked as inclusion bodies (IB).
The denatured chimeric proteins in 6M urea were filtrated, then 10 mM imidazole was added. The protein was subjected to immobilized metal affinity chromatography using 5 ml His-Trap columns, then eluted with a linear imidazole gradient of 10–500 mm (**Part 2, Figure 4**, rightmost panel). Calibration experiments were performed to allow binding of the fusion protein to the affinity column (not shown). **Figures 4 and 5 (Part 2)** shows affinity purification of the TAT-MTS-PiC-A fusion protein. A key element for the binding to the affinity column was using NaH_2PO4 in the binding buffer.
Next, the buffer was exchanged to a physiological one, to allow the TAT-PIC fusion proteins to be tested in biological systems. Calibration experiments helped to define the dialysis buffer: the buffer needed to contain 200 mM L-Arginine (**Part 2, Figure 6**). **Figure 7** summarizes the calibration experiments for purification of TAT-MTS-mPiC-A. The same procedure was used to purify TAT-PiC-B (**Part 2, Figure 8**).
Sub-task was fully accomplished.
5) Testing correct targeting in mitochondria isolated from mice with SkM PiC loss (Aim 3).

This was not done. The world-wide pandemic caused major interruptions in lab work, especially in Israel, where Aim 3 was performed. To undertake this sub-task, we would have had to ship TAT fusion protein from Israel to Philadelphia, or the PiC mice from Philadelphia to Israel. Another unfortunate outcome of the pandemic was that shipping of biological materials (namely, the fusion proteins, or mice, between Philadelphia and Israel) became unreliable.

Sub-task was not performed.

6) Testing correct targeting in cell cultures (immortalized MEFs, myoblasts, HEK-PiC(-/-) cells) (Aim 3).

To determine if TAT-MTS-PiC-A localized correctly to the inner mitochondrial membrane of mitochondria, as a first step we incubated HeLa cells with TAT-MTS-PiC-A for 3 hr, prepared lysates from control (untreated cells) or treated cells, and evaluated the expression the fusion protein using anti-PiC antibodies. **Part 2, Figure 10** shows that the fusion protein was found in the cell lysates, in proportion to the amount that was added (dose response). Thus, TAT-MTS-PiC-A is successfully internalized into cells.

Next, to determine if TAT-MTS-PiC-A localized correctly to the inner mitochondrial membrane (IMM) of mitochondria, HeLa cells were incubated with TAT-MTS-PiC-A for 3 hr and sub-fractionation was performed (sub-fractionation shown in **Part2, Figure 11**). Fusion protein expression was tested by

western blot using an anti-PiC antibody. Purity of the sub-fractions was determined using anti-Tubulin antibodies for the cytosolic sub-fraction, anti-Lamin B antibodies for the nucleus and anti-CoIV for the IMM sub-fraction. As seen in **Figure 12**, TAT-MTS-PiC-A localized to the IMM, with no evidence for expression in the mitochondrial matrix or outer mitochondrial membrane. We repeated these experiments using 3 different cell types (Hela cells, HEK293 cells and HePG2 cells), with the same outcome (**Part 2, Figure 13)**.

Sub-task was fully accomplished.

7) Labeling fusion proteins with fluorescent dye (FITC) and testing localization to mitochondria (Aim 3).

This experiment was not performed because the sub-fractionation studies (Part 2, Figure 10-13) clearly demonstrated that TAT-PiC-A localized to the IMM. Furthermore, the fluorescence labeling would allow for discrimination between IMM, matrix and OMM; therefore, the sub-fractionation studies are more accurate.

Sub-task was not performed.

Major Task 2 – Parts of Specific Aims 2 and 3B

1) Human primary muscle cells: Calcium flux studies (cytosolic and mitochondrial Ca^{2+}), western blot analysis and qPCR. (Aim 2)

We used HEK293 cells with CRISPR knockout of PiC; several clones were tested for PiC expression (knockout was confirmed by western blot). Cytoplasmic Ca^{2+} signaling was evaluated in these clones compared to control cells.. These data were presented in Progress Report 2018. We obtained largely negative data, despite many attempts and changes of experimental design. Consequently, we focused our efforts to the mouse studies.

Sub-task was fully accomplished.

2) Isolated mitochondria from PiC-HSA-Cre+ and PiC-Cre- mice: mitochondrial Ca^{2+} uptake and clearance studies (Aim 2).

To evaluate the relevance of PiC for mitochondrial Ca^{2+} handling, isolated skeletal muscle (SM) mitochondria were prepared. We first determined if PiC-depleted mitochondria were competent to take up Ca^{2+}, by measuring the clearance of a $CaCl_2$ pulse from the incubation medium, using Fura-lowAff to measure Ca^{2+}, and in the presence of CGP37157 to inhibit mitochondrial Ca^{2+} efflux across the Na^+/Ca^{2+} exchanger. Mitochondria were first depleted of endogenous Pi by incubation with glucose, hexokinase and ADP, pelleting, then resuspending mitochondria in incubation medium devoid of these components. Using mitochondria energized with P/M, the concentration of Ca^{2+} in the buffer ($[Ca^{2+}]c$) was measured 30 seconds after a 10 μM $CaCl_2$ addition. PiC KD (knockdown) mitochondria not only were capable of taking up Ca^{2+}, the clearance at 30 seconds was 37% greater compared to Control (Ctrl) mitochondria (**Part 1, Figure 2A**). Ca^{2+} clearance was Ruthenium Red (RuR)-dependent in both genotypes, indicating that clearance was mediated by the mitochondrial calcium uniporter (mtCU) (**Figure 2A**).

To determine the concentration of free Ca^{2+} in the mitochondrial matrix ($[Ca^{2+}]m$), SM mitochondria were loaded with Fura-FF, then incubated under the conditions used to determine Ca^{2+} clearance. Upon addition of 10 μM $CaCl_2$ to the incubation medium, $[Ca^{2+}]m$ rose in mitochondria from both genotypes, but the increase was ~80% larger in PiC KD mitochondria (**Figure 2B**). The rise in $[Ca^{2+}]m$ in both genotypes was RuR-dependent and thus mtCU-mediated. To determine if the greater increase in $[Ca^{2+}]m$ in PiC KD mitochondria was due to the greater uptake of Ca^{2+}, we determined a concentration of RuR that would partially suppress Ca^{2+} uptake in PiC KD

mitochondria, with the goal of minimizing the difference in Ca^{2+} clearance between PiC KD and Ctrl preparations. This was achieved using the submaximal dose of 5 nM RuR (**Figure 2C**). When $[Ca^{2+}]m$ was compared in Ctrl and ko preparations that cleared Ca^{2+} to a similar extent, $[Ca^{2+}]m$ was still substantially higher in ko mitochondria (**Figure 2D**).

Sub-task was fully accomplished.

3) Testing Functionality of TAT-PiC using ^{32}Pi transport in isolated mito (Aim 3).

Experiments using ^{32}Pi were not performed. Instead, the functionality of the PiC delivered using the TAT fusion protein was evaluated using bioenergetics studies (**Part 2, Figure 16**), and phosphate concentrations (**Part 2, Figure 18**).

Sub-task was not accomplished as described, however experiments shown in the indicated figures accomplished the same goal (and avoided the use of radioactivity).

4) Testing lack of deleterious effects of delivering TAT-PiC in cells; testing if TAT-PiC fusion proteins kills cells, slows proliferation, depletes ATP, decreases ETC capacity, increases ETC leakiness, causes abnormal mitochondrial Ca^{2+} uptake, or causes mitochondrial fragmentation or hyperfusion indicative of cell stress (Aim 3).

To determine if TAT-MTS-PiC-A/B chimeric proteins (and the suspension buffer) can be used in biological system, we exposed HeLa cells to TAT-PiC-A and determined cell viability as compared to control cells exposed to buffer only. As shown in **Part 2, Figure 9**, TAT-MTS-PiC-A had no cytotoxic effect on HeLa cells. This was tested for several concentrations of the fusion protein.

Proliferation, bioenergetics (ETC (electron transport chain) capacity) were determined as part of the series of experiments that tested the use of TAT-PIC to rescue cells in which PiC expression was decreased (see Major Task 3, sub-task 1, below).

Studies of mitochondrial Ca^{2+} flux and mitochondrial fragmentation/hyperfusion were not conducted. Decreased accessibility to the lab due to restrictions imposed by the pandemic forced us to prioritize experiments. Cell viability and rescue experiments were prioritized, over Ca^{2+} and mitochondrial morphology studies in the context of the TAT-PiC chimeric proteins.

Sub-task was partially accomplished.

Major Task 3 – Aim 1, Part of Aim 3.

1) Testing rescue of PiC loss phenotypes: we will compare cell/mitochondria/mice with PiC depletion and after rescue with TAT-PiC, to determine if TAT-PiC can restore normal oxphos, cell proliferation in cell cultures and exercise capacity in the mouse model (Aim 3).

We next tested the ability of TAT-MTS-PiC-A to rescue mitochondrial function in cells with decreased expression of PiC using siRNA. Transient transfection of Hela cells with si-PiC lowered PiC mRNA levels by more than 85%, as determined by qPCR (**Part 2, Figure 14**). Transfected cells, at 48 hr post transfection, grew slower, with a 43% decrease in cell number (**Part 2, Figure 15A, B**). Treatment with TAT-MTS-PiC-A for 24 hr increased the cell proliferation rate (~15% higher cell number by the end of the incubation period) (**Part 2, Figure 15A, B**).

We next tested the effect of TAT-MTS-PiC-A mitochondrial bioenergetics in Hela cells with decreased expression of PiC (**Part 2, Figure 16**). Treatment with TAT-MTS-PiC-A fusion protein

significantly improved mitochondrial bioenergetics (measured as O_2 consumption rate), showing a 3x increase with 10 µg of fusion protein and 9.3x increase after treatment with 20 µg of the fusion protein. Treatment with the fusion protein also increased ATP production; 1.8x and 3.3x with 10 µg and 20 µg of the fusion protein respectively (**Figure 16**).

Additionally, cells with defective oxidative phosphorylation often increase their reliance on glycolysis, with conversion of pyruvate to lactate to regenerate NAD^+. Lactate levels were measured in the medium of cells cultured in 25 mM glucose. Lactate levels increased upon knockdown of PiC, by 1.9 fold. Levels decreased to WT levels when PiC knockdown cells were treated with TAT-PiC-A (**Part 2, Figure 17**).

We further tested the efficacy of TAT-PiC-A to rescue phenotypes in HeLa cells with PiC knockdown, by measuring total cellular phosphate concentration. PiC knockdown resulted into a substantially lower total cellular phosphate (**Part 2, Figure 18**). Treatment with TAT-PiC-A dose-dependently increased phosphate levels, with the highest concentration of TAT-PiC resulting in a phosphate level similar to that observed in control cells.

Finally, it was reported that the PiC also transports copper (Boulet et al 2018 PMID 29237729). PiC was knocked down in Hela cells using si-RNA, then treated with 30µg TAT-MTS-PiC-A protein. Copper concentration was determined in mitochondria. Cu levels decreased to 75% upon PiC knockdown, then were restored, to 119% of control level, when PiC knockdown cells were treated with 30µg TAT-PiC-A (**Part 2, Figure 19**).

Sub-task was fully accomplished.

2) Testing rescue of PiC loss phenotypes: we will compare cell/mitochondria/mice with PiC depletion and after rescue with TAT-PiC, to determine if TAT-PiC can restore normal oxphos, cell proliferation in cell cultures and exercise capacity in the mouse model (Aim 3).

This was not performed. The world-wide resulted in major disruptions of lab work, especially in Israel (where this sub-task would have been performed). Furthermore, to undertake this sub-task, we would have had to ship PiC mice from Philadelphia to Israel, and another unfortunate outcome of the pandemic was that shipping of biological materials became unreliable. Therefore, we opted not to pursue this sub-task.

Sub-task was not performed.

3) Physiology: breathing, ex vivo skeletal muscle and diaphragm, muscle histology (site 2), plus analysis (Aim 1).

Given the role of cytoplasmic Ca^{2+} in cross-bridge cycling and the suppressed cytoplasmic Ca^{2+} response to repetitive tetanic stimulation (RTS) in PiC-depleted muscle, we tested skeletal muscle force generation *ex vivo* using extensor digitorum longus (EDL) muscle challenged with a single twitch (ST) and RTS stimulation. We first note that muscle cross-sectional area (CSA) did not differ between Ctrl and PiC KD EDL (**Part 1, Figure 6A**), consistent with the similar quadriceps weight in both genotypes (**see Part 1, Figure 1B**). With ST stimulation, CSA-normalized force generated by PiC-depleted EDL trended lower (**Figure 6B**), with no change in the rate of force development (**Figure 6C**), though time-to-peak was slightly (~20%) but consistently faster (**Figure 6D**). With the RTS protocol, there was again a tendency for lesser force generation by PiC-depleted EDL (**Figure 6E**), and, again, with no difference in the rate of force development (**Figure 6F**). However, the time-to-peak was significantly and substantially delayed, by a factor of ~2, in PiC-depleted EDL (**Figure 6G**); this is consistent with the lower $[Ca^{2+}]c$ rise in PiC-depleted EDL in response to a tetani (**see**

Part 1, Figure 5C).
Breathing was not evaluated because the post-doctoral fellow at University of Pennsylvania with the relevant expertise left to take an industry job in the U.K., then, shortly thereafter, labs were closed due to the pandemic. The expertise was not recovered in the lab at U. Pennsylvania.

Sub-task was partially accomplished (the breathing studies were omitted).
Major Task 4 – Part of Specific Aim 2

1) Ca^{2+} uptake studies in isolated skeletal muscle mitochondria, and expression of mito Ca2+ uptake proteins in mitochondria (Aim 2)

Ca2+ uptake studies in isolated mitochondria were described in Major Task 2, sub-task 2, above.

Expression of mitochondrial Ca^{2+} uptake proteins: Since PiC KD mitochondria exhibited greater RuR-inhibitable Ca^{2+} uptake (see **Part 1, Figure 2**), we questioned whether PiC-depleted mitochondria had a greater mitochondrial Ca^{2+} uniporter (mtCU) capacity. To investigate this, protein levels of the mtCU components were evaluated in the mitochondrial preparations used for the Ca^{2+} flux studies. Immunoblotting revealed that protein expression of MCU, EMRE and MICU1 were elevated by ~50% in KD mitochondria when compared to aconitase (ACO2), and also to TOM20 (**Part 1, Figure 4A**). That the increase in expression of each mtCU component was similar in PiC-depleted mitochondria suggested a greater abundance of the functional mtCU complex. To better evaluate if expression of the mtCU complex was increased, we determined the abundance of the native complex. To this end, samples of mitochondria were electrophoresed under non-denaturing conditions, then a second-dimension gel was run under denaturing conditions and probed with antibodies against MCU and EMRE. MCU and EMRE immunoreactive bands corresponded to complexes of ~750 kDa and ~1000 kDa molecular weight (MW), and were detected in both Ctrl and KD samples, though at higher abundance in KD mitochondria (**Part 1, Suppl Fig. 3B, C**). This experiment was repeated in a second pair on Ctrl and KD mitochondria, and had a similar outcome (not shown). Note that the Coomassie-stained gel (**Suppl. Figure 3A**), and also the Complex II subunit SDHA (**Suppl. Figure 3D**), serve as loading controls. An MCU-immunoreactive complex of ~1100 kDa was detected in cortical neurons (which also abundantly express MICU1 and MICU3), and an ~750-800 kDa complex immunoreactive for MCU was detected in heart mitochondria which expresses relatively low amounts of MICU1. Low EMRE expression can lead to the accumulation of lower MW MCU-immunoreactive mtCU intermediates. To determine if such an intermediate can be detected with our approach, and, thus, to demonstrate that an mtCU intermediate was detectable, we repeated the same electrophoresis protocols using skeletal muscle mitochondria from mice depleted of MICU1 in striated muscle and floxed control mice. This model of skeletal muscle depletion of MICU1 shows substantial loss of EMRE protein and some loss of MCU protein. Electrophoresis under native followed by denaturing conditions resulted in only an MCU immunoreative band corresponding to a ~480 kDa complex in MICU1-depleted mitochondria but were no MCU immunoreactive bands corresponding to higher MW complexes (**Suppl. Figure 3E**). In contrast, the control sample showed similar immunoreative bands corresponding to higher MW complexes (**Suppl. Figure 3E**) as observed in PiC KD and Ctrl mitochondria (**Suppl. Figure 3B**). Substantial loss of EMRE is also evident in the MICU1-depleted sample (**Suppl. Figure 3F**) whereas EMRE is present in the Ctrl sample (**Suppl. Figure 3F**). The appearance of the MCU-immunoreactive band associated with a lower MW complex in MICU1-depleted samples is similar to what was observed in HeLa cells lacking MICU1 and EMRE. Overall this analysis is consist with a greater abundance not only of components of mtCU in PiC KD mitochondria but of the assembled mtCU complex.
To evaluate MCU abundance at the level of the whole muscle (as a surrogate for mtCU capacity at the whole muscle level), immunoblotting was repeated in quadriceps lysates, with α-tubulin as the loading control. For comparison, mitochondrial proteins from the outer mitochondrial membrane

(TOM20), and matrix (ACO2 and TFAM) were also we detected. All mitochondrial proteins were increased in KD quadriceps, suggesting a generalized increase in the abundance of mitochondria (**Part 1, Figure 4B**). We noted that, compared to the other mitochondrial proteins, the increase in MCU in KD quadriceps was ~2x higher. In summary, these data suggest that isolated KD mitochondria have a ~50% greater mtCU capacity, and that mtCU capacity may be even more expanded (~2x) at the level of the whole muscle.
Sub-task was fully accomplished.

2) Mouse fibers: Ca^{2+} flux studies (cytoplasmic and mitochondrial), membrane potential determination, NADPH autofluorescence (Aim 2)

Membrane potential studies: Because mitochondrial membrane potential ($\Delta\Psi_m$) is inextricably linked to mitochondrial Ca^{2+} uptake, $\Delta\Psi_m$ was evaluated using TMRM (tetramethyl rhodamine esthyl ester), and done simultaneously with the Ca^{2+} clearance measurements. Energizing mitochondria with P/M prior to $CaCl_2$ addition polarized $\Delta\Psi_m$ to the same extent in Ctrl and KD mitochondria (Fig. 3A). In response to a 10 μM $CaCl_2$ bolus, some depolarization was noted in both genotypes, but the magnitude was consistently greater in KD mitochondria (**Part 1, Figure 3A**). Though this greater $\Delta\Psi_m$ response in PiC-depleted mitochondria might be explained by the lack of, or lesser, matrix acidification, other mechanisms were possible. In particular, we questioned whether residual ADP (e.g., from the Pi depletion reaction) combined with the greater matrix free Ca^{2+}, and the observation that KD mitochondria retained some capacity for oxphos, might actually lead to a greater stimulation of oxphos in KD than in Ctrl mitochondria. This was tested by measuring $\Delta\Psi_m$ during the $CaCl_2$ bolus in the presence of oligomycin to inhibit the ATP synthase. Oligomycin addition caused both KD and Ctrl mitochondria, energized with P/M, to hyperpolarize (**Figure 3B**), indicating that in both Ctrl and KD mitochondria some oxphos was occurring in the absence of oligomycin. Addition of 10 μM $CaCl_2$ once again caused both KD and Ctrl mitochondria to depolarize. This again occurred to a greater extent in KD mitochondria (**Figure 3B**), indicating that the larger depolarization in PiC-depleted mitochondria cannot be explained by a greater Ca^{2+}-dependent stimulation of oxphos.
Ca^{2+} flux studies in muscle fibers: Considering the ability of skeletal muscle (SM) mitochondria to buffer Ca^{2+} released from the sarcoplasmic reticulum (SR), we evaluated the impact of PiC depletion in SM on cytoplasmic Ca^{2+} transients. This was done in flexus digitorum brevis (FDB) fibers during single twitch (ST) or repeated tetanic stimulation (RTS), performed sequentially in each FDB preparation. Baseline $[Ca^{2+}]_c$ (cytoplasmic Ca^{2+} concentration) before each stimulus paradigm was similar between KD and Ctrl fibers (**Part 1, Figure 5A**). The ST stimulation evoked a similar ~50 nM cytoplasmic Ca^{2+} transient in fibers from both genotypes (**Figure 5A, B**), that decayed with a similar kinetic (**Part 1, Suppl. Figure 4**). When the RTS protocol was tested, Ctrl (Control) fibers responded with a rapid-onset, substantial and sustained rise in $[Ca^{2+}]c$. $[Ca^{2+}]c$ continued to increase throughout the stimulation period, though with a slower kinetic (**Figure 5A, C**). Fibers depleted of PiC responded with the same pattern of cytoplasmic Ca^{2+} elevation, but with two differences. First, the rising phase tended to be faster in KD fibers (**Figure 5A**). Second, the amplitude of the $[Ca^{2+}]c$ rise was less in KD fibers, at both the onset and the end of the stimulation period (**Figure 5A**); the maximal rise in $[Ca^{2+}]c$ was significantly lower, by ~30% (**Figure 5C**).
To gain insight into the lower amplitude response to RTS in KD fibers, protein levels of ER Ca^{2+} handling proteins were evaluated by immunoblotting in lysates from quadriceps muscle. KD and Ctrl muscle showed similar protein expression of the type 1 ryanodine receptor (RyR1) Ca^{2+} release channel, and the Ca^{2+}-binding proteins calsequestrin (CASQ1) and calreticulin (CALR) (**Figure 5D**). Expression of the main SR Ca^{2+} uptake protein in skeletal muscle, SERCA1, was slightly (~20%) but significantly decreased in KD muscle, as was the protein level of the major skeletal muscle subunit of the L-type Ca^{2+} channel (CAV1.1) (**Figure 5D**). These protein expression data indicate that the lower $[Ca^{2+}]c$ response to RTS in KD fibers cannot be explained by changes in the abundance of ER Ca^{2+} release channels. Furthermore, the similar decay kinetic in KD and Ctrl fibers following RTS suggests that the small decrease in SERCA1 expression was unlikely of functional

relevance.
Because mitochondrial myopathies are progressive, we were interested to determine if there was a progression in any aspect the Ca^{2+} phenotype in PiC KD mice. To this end, we repeated the RTS protocol in FDB fibers and immunoblot detection of Ca^{2+} handling proteins in muscle from older mice. In FDB fibers, resting $[Ca^{2+}]c$ was similar in Ctrl and KD preparations (**Part 1, Figure 7C**), and also similar to levels observed in younger mice. With RTS, the $[Ca^{2+}]c$ response in FDB from older Ctrl mice showed a pattern similar to that measured in younger Ctrl mice, though with a slightly elevated amplitude (**Figure 7C, compared to Figure 5A,C**). In contrast, PiC-depleted FDB from older mice responded to RTS with a $[Ca^{2+}]c$ rise that was slower in onset compared to the Ctrl response, and with a ~70% lower amplitude (**Figure 7C**). Immunoblotting of muscle lysates showed a continued higher expression of all mtCU components in KD muscle from older mice, at levels similar to younger KD mice, along with unchanged levels of ER Ca^{2+} binding proteins, SERCA1 and Cav1.1 relative to Ctrl levels. However, muscle from older KD mice showed a substantial decrease in RyR1 protein expression, by ~50% (**Figure 7D**), consistent with the dramatically suppressed $[Ca^{2+}]c$ rise during RTS in muscle from 22-24 week-old PiC KD mice.
NADPH autofluorescence was measured, however data were not included in the Report because, based on the control data, we could not obtain a substantial enough dynamic range to be able to detect changes should there be any in the PiC KD model.
Sub-task was fully accomplished (though NADPH data were deemed unreliable and not included in the manuscript).

Accomplishments, described in manuscript form

Part 1: A partial manuscript, that includes a complete data set and description of the results, as well as Introduction and Methods sections, covering Aims 1 and 2. Missing are the Abstract and Discussion.

Part 2: A complete data set of work on Aim 3 is presented after the abovementioned partial manuscript.

PART 1

Abundant mitochondrial Ca^{2+} uptake despite substantial depletion of the mitochondrial phosphate carrier in skeletal muscle

Cesar Vasquez-Trincado[1], Arijita Gosh[1], Ji In Han[1], Valentina Debattisti[1], Carmen Bekeova[1], Emanuele Loro[2], Tejvir Khurana[2], Gyorgy Hajnoczky[1*], Erin L. Seifert[1*]

1. Department of Pathology, Anatomy and Cell Biology and MitoCare Center, Thomas Jefferson University, Philadelphia PA 19107
2. Department of Physiology, University of Pennsylvania, Philadelphia, PA 19004

Running title: Mitochondrial Ca^{2+} handling in PiC-deficient muscle

*Correspondence:

Erin L. Seifert, Ph.D.
Associate Professor
Department of Pathology, Anatomy and Cell Biology,
MitoCare Center for Mitochondrial Imaging Research and Diagnostics
1020 Locust Street, Suite 527
Thomas Jefferson University,
Philadelphia PA 19107
Erin.Seifert@Jefferson.edu
and
György Hajnóczky, M.D., Ph.D.
Professor
Department of Pathology, Anatomy and Cell Biology,
MitoCare Center for Mitochondrial Imaging Research and Diagnostics
1020 Locust Street, Suite 527
Thomas Jefferson University,
Philadelphia PA 19107
Gyorgy.Hajnoczky@Jefferson.edu

ABSTRACT

INTRODUCTION

That mitochondria can take up a tremendous amount of Ca^{2+} has been known for a long time (McCormack, Halestrap et al., 1990). The molecular identification of the uniporter was more recently discovered, and revealed to be a hetero-oligomeric complex (mtCU) formed by a pore forming subunit, MCU (Baughman, Perocchi et al., 2011, De Stefani, Raffaello et al., 2011), a scaffold required for function, EMRE (Sancak, Markhard et al., 2013), and regulatory subunits (MICUs:

MICU1/2/3) (Csordas, Golenar et al., 2013, Mallilankaraman, Cardenas et al., 2012, Patron, Raffaello et al., 2013, Perocchi, Gohil et al., 2010, Plovanich, Bogorad et al., 2013). MCU paralog, MCUb, may also be present and produce a dominant negative phenotype (Raffaello, De Stefani et al., 2013). The discovery of mtCU provided the opportunity to gain insight into the relevance of mitochondrial Ca^{2+} uptake in physiological and pathological settings. Different mouse models of the mtCU components have, to a greater or lesser extent, indicated that mitochondrial Ca^{2+} uptake and its regulation are relevant in several *in vivo* contexts (reviewed in: (Modesti, Danese et al., 2021)), such as in skeletal muscle (Debattisti, Horn et al., 2019, Gherardi, Nogara et al., 2019, Kwong, Huo et al., 2018, Mammucari, Gherardi et al., 2015, Pan, Liu et al., 2013). Relevance of the mtCU in humans has been demonstrated by loss-of-function variants in the main mtCU regulatory subunit, MICU1, associated with neuromuscular phenotypes (Lewis-Smith, Kamer et al., 2016, Logan, Szabadkai et al., 2014, Musa, Eyaid et al., 2019), and a variant in MICU2 that is associated with neurodevelopmental abnormalities (Shamseldin, Alasmari et al., 2017). While the mechanism whereby mitochondrial Ca^{2+} uptake alters complex phenotypes is likely to be cell type-specific, possible paradigms include the enhancement of substrate metabolism in the matrix via stimulation of Ca^{2+}-sensitive matrix proteins (Glancy & Balaban, 2012, McCormack et al., 1990), and the alteration of Ca^{2+} signals, and their targets, in other compartments (Eisner, Csordas et al., 2013).

A feature of mitochondrial Ca^{2+} uptake that is equal in importance to the protein machinery is the requirement for the membrane potential ($\Delta\Psi m$) across the inner mitochondrial membrane as a driving force (Lehninger, 1974, Nicholls, 2005). While this utilization of $\Delta\Psi m$ could leave mitochondrial Ca^{2+} uptake vulnerable to self-imposed $\Delta\Psi m$ dissipation, run-down can be prevented by co-transport of a weak acid, suggesting that uptake of a weak acid is also required for sustained mitochondrial Ca^{2+} uptake (Nicholls, 2005). A readily available endogenous source of weak acid is provided by the transport of inorganic phosphate (Pi) by the PiC into the mitochondrial matrix (Nicholls, 2005). PiC, encoded by SLC25A3, transports Pi as H_3PO_4 uniport or as $H_2PO_4^-/OH^-$ antiport (reviewed in: (Seifert, Ligeti et al., 2015)), which would supply H^+ to (re)acidify the matrix, leading to (re)establishment of $\Delta\Psi m$ and thus allowing mitochondrial Ca^{2+} uptake to continue without the constraint of major $\Delta\Psi m$ loss. The matrix swelling that would result from the uptake of a weak acid into the mitochondrial matrix can be mitigated by the formation of osmotically-inert amorphous solids of phosphorus and Ca^{2+} (Chalmers & Nicholls, 2003, Lehninger, 1974, Wolf, Mutsafi et al., 2017).

The foregoing suggests that Ca^{2+} uptake by the mtCU and the concentration of free Ca^{2+} in the mitochondrial matrix would be inextricably linked to Pi uptake by the PiC. Yet, whether, or the extent,

to which mitochondrial Ca^{2+} depends on the PiC has not been explicitly tested. Furthermore, beyond the basic biology of mitochondrial Ca^{2+} uptake, understanding its dependence on the PiC may be relevant for human disease. Notably, homozygous pathogenic variants in SLC25A3 resulting in loss of the major PiC isoform in striated muscle cause skeletal myopathy (Mayr, Merkel et al., 2007, Mayr, Zimmermann et al., 2011), and mtCU current density and MCU expression are especially high in skeletal muscle (Fieni, Lee et al., 2012, Paillard, Csordas et al., 2018). The latter also indicates that skeletal muscle would be a particularly interesting context for investigating the dependence of mitochondrial Ca^{2+} uptake and matrix Ca^{2+} buffering on the PiC. To this end, we generated mice with skeletal muscle-specific depletion of the PiC. Young adult mice with PiC depletion in skeletal muscle were healthy and without the atrophy described in several mouse models of primary mitochondrial dysfunction in skeletal muscle (Favaro, Romanello et al., 2019, Tezze, Romanello et al., 2017, Touvier, De Palma et al., 2015), thus providing a model that was devoid of major pathology. These young adult PiC-depleted mice did however display a mild decrease in running capacity, which progressed to an extreme exercise intolerance, providing the opportunity to also gain insight into cellular Ca^{2+} dynamics in PiC-depleted skeletal muscle in the context of a severe functional defect.

RESULTS

Model of skeletal muscle-specific PiC depletion

Our goal was to generate mice with inducible depletion of PiC in skeletal muscle. To this end, mice harboring floxed PiC alleles ($PiC^{fl/fl}$) (Kwong, Davis et al., 2014) were crossed with mice expressing the double fusion protein comprising MerCreMer and the Human Skeletal Actin promoter (HSA-MCM) (McCarthy, Srikuea et al., 2012) to generate mice with skeletal muscle-specific Tamoxifen (Tam)-inducible PiC loss. HSA-MCM-$PiC^{fl/fl}$ and $PiC^{fl/fl}$ mice were treated with Tamoxifen (Tam) for 4 days starting at 9 weeks of age. Immunoblot evaluation of PiC protein expression revealed that PiC was decreased by 90-95% in most muscles (Fig. 1A). We however noticed that HSA-MCM-$PiC^{fl/fl}$ mice that were not treated with Tam also showed substantial depletion of PiC in skeletal muscle. The colony was subsequently re-derived using new founders, but the outcome was the same. HSA-MCM mice in our colony that were crossed with other floxed models showed the expected Tam-dependence (not shown), and HSA-MCM-$PiC^{wt/wt}$ mice showed similar levels of PiC protein in skeletal muscle as $PiC^{fl/fl}$ mice. Thus, the Tam-independent PiC loss was likely a peculiarity of the HSA-MCM-$PiC^{fl/fl}$ model. Importantly, we noted that PiC was depleted in skeletal muscle and not in heart, whole brain, liver, or kidney (Suppl. Fig. 1). Furthermore, HSA-MCM-$PiC^{fl/fl}$ mice were born at/higher than the expected Mendelian ratio (41% Cre-, 59% Cre+; 11 litters, 93 mice), remained healthy well into adulthood (see below), and mortality was not observed in mice as

old as 1 year of age. We determined that 4 days of Tam treatment further decreased PiC protein in skeletal muscle. Thus we systematically treated 9-week-old HSA-MCM-PiC$^{fl/f}$ mice and control PiC$^{fl/fl}$ mice with Tam; these mice will be referred to as PiC KD and Ctrl mice, respectively.

Several models of mitochondrial dysfunction in skeletal muscle resulted in myopathy characterized by deteriorating muscle and body mass, and early mortality (Favaro et al., 2019, Pereira, Tadinada et al., 2017, Tezze et al., 2017, Touvier et al., 2015). Because we aimed to evaluate mitochondrial Ca^{2+} handling and cytosolic Ca^{2+} dynamics without concurrent pathology, we screened PiC KD mice for body weight and lean mass, and identified 13 wks of age (3 wks post-Tam) as a time point when body and skeletal muscle weight, and also white adipose tissue weight were similar in PiC KD and Ctrl mice. This time point also allowed for Tam washout (Fig. 1B). Unless otherwise indicated, experiments were conducted using mice at this time point (i.e., 3 weeks after the final Tam injection corresponding to 13 weeks of age), with PiC depletion in different muscles as shown in Fig. 1A.

PiC is the predominant, or only, source of Pi for ATP synthesis by oxidative phosphorylation (oxphos); thus we expected that substantial PiC depletion in skeletal muscle would strongly limit oxphos. To determine if PiC-depleted mitochondria exhibited this expected bioenergetics defect, bioenergetics analyses were performed using mitochondria isolated from all limb muscles and energized with pyruvate and malate (P/M). Substrate oxidation was evaluated as O_2 consumption rate (JO_2). Maximal oxphos (saturating P/M and ADP) was ~75% lower in PiC KD mitochondria, whereas JO_2 in the presence of oligomycin (ATP synthase inhibition), which measures maximal non-phosphorylating (leak) JO_2, was similar between KD and Ctrl mitochondria (Fig. 1C). Together, these observations are consistent with a Pi limitation on oxphos in PiC-depleted mitochondria. This limitation was severe; in PiC KD mitochondria, maximal phosphorylating JO_2 was 2x higher than the non-phosphorylating rate, compared to ~10.5x higher in Ctrl mitochondria. We noted that the maximal uncoupled JO_2 (+FCCP) was significantly higher in KD mitochondria (Fig. 1C), indicating a greater electron transport chain capacity. The latter likely reflects a secondary upregulation of mitochondrial proteins, documented in other mouse models and in cell from humans with deficient oxphos (Dogan, Cerutti et al., 2018, Havlickova Karbanova, Cizkova Vrbacka et al., 2012, Joseph, Rungi et al., 2004, Kovarova, Cizkova Vrbacka et al., 2012, Viscomi, Bottani et al., 2011), rather than a primary defect caused by PiC depletion. Thus mitochondria having a >90% depletion of the PiC exhibited the expected Pi limitation of oxphos, and this limitation prevented most of the phosphorylating component of JO_2.

Increased mitochondrial Ca^{2+} uptake in PiC-depleted mitochondria

To evaluate the relevance of PiC for mitochondrial Ca^{2+} handling, isolated skeletal muscle

mitochondria were prepared as for the JO_2 experiments. We first determined if PiC-depleted mitochondria were competent to take up Ca^{2+}. This was evaluated by measuring the clearance of a $CaCl_2$ pulse from the incubation medium, using Fura-lowAff to measure Ca^{2+}, and in the presence of CGP37157 to inhibit mitochondrial Ca^{2+} efflux across the Na^+/Ca^{2+} exchanger. In addition, mitochondria were first depleted of endogenous Pi by incubation with glucose, hexokinase and ADP, pelleting, then resuspending mitochondria in incubation medium devoid of these components (Chalmers & Nicholls, 2003). Using mitochondria energized with P/M, the concentration of Ca^{2+} in the buffer ($[Ca^{2+}]c$) was measured 30 seconds after a 10 μM $CaCl_2$ addition. PiC KD mitochondria not only were capable of taking up Ca^{2+}, the clearance at 30 seconds was 37% greater in KD compared to Ctrl mitochondria (Fig. 2A). Ca^{2+} clearance was Ruthenium Red (RuR)-dependent in both genotypes, indicating that clearance was mediated by the mtCU (Fig. 2A).

To determine the concentration of free Ca^{2+} in the mitochondrial matrix ($[Ca^{2+}]m$), isolated skeletal muscle mitochondria were loaded with Fura-FF (see Methods), then incubated under the conditions used to determine Ca^{2+} clearance. Upon addition of 10 μM $CaCl_2$ to the incubation medium, $[Ca^{2+}]m$ rose in mitochondria from both genotypes, but the increase was ~80% larger in KD mitochondria (Fig. 2B). The rise in $[Ca^{2+}]m$ in both genotypes was RuR-dependent and thus mtCU-mediated. To determine if the greater increase in $[Ca^{2+}]m$ in KD mitochondria might simply be due to the greater uptake of Ca^{2+}, we determined a concentration of RuR that would partially suppress Ca^{2+} uptake in KD mitochondria with the goal of minimizing the difference in Ca^{2+} clearance between KD and Ctrl preparations. This was achieved using the submaximal dose of 5 nM RuR (Fig. 2C). When $[Ca^{2+}]m$ was compared in Ctrl and KD preparations that cleared Ca^{2+} to a similar extent, $[Ca^{2+}]m$ was still substantially higher in KD mitochondria (Fig. 2D).

PiC KD mitochondria depolarize more upon Ca^{2+} uptake

Because $\Delta\Psi_m$ is inextricably linked to mitochondrial Ca^{2+} uptake, $\Delta\Psi_m$ was evaluated using TMRM, and done simultaneously with the Ca^{2+} clearance measurements. Energizing mitochondria with P/M prior to $CaCl_2$ addition polarized $\Delta\Psi_m$ to the same extent in Ctrl and KD mitochondria (Fig. 3A). In response to a 10 μM $CaCl_2$ bolus, some depolarization was noted in both genotypes, but the magnitude was consistently greater in KD mitochondria (Fig. 3A). Though this greater $\Delta\Psi_m$ response in PiC-depleted mitochondria might be explained by the lack of, or lesser, matrix acidification, other mechanisms were possible. In particular, we questioned whether residual ADP (e.g., from the Pi depletion reaction) combined with the greater matrix free Ca^{2+}, and the observation that KD mitochondria retained some capacity for oxphos, might actually lead to a greater stimulation of oxphos in KD than in Ctrl mitochondria. This was tested by measuring $\Delta\Psi_m$ during the $CaCl_2$ bolus in the presence of oligomycin to inhibit the ATP synthase. Oligomycin addition caused both KD and Ctrl mitochondria, energized with P/M, to hyperpolarize (Fig. 3B), indicating that in both Ctrl

and KD mitochondria some oxphos was occurring in the absence of oligomycin. Addition of 10 µM $CaCl_2$ once again caused both KD and Ctrl mitochondria to depolarize. This again occurred to a greater extent in KD mitochondria (Fig. 3B), indicating that the larger depolarization in PiC-depleted mitochondria cannot be explained by a greater Ca^{2+}-dependent stimulation of oxphos. Considering that PiC and/or P_i may regulate the permeability transition pore (PTP) (Basso, Petronilli et al., 2008, Crompton & Costi, 1988, Leung, Varanyuwatana et al., 2008, Varanyuwatana & Halestrap, 2012), we also tested whether the greater Ca^{2+}-dependent depolarization in KD mitochondria was related to PTP opening. Measurements of $\Delta\Psi_m$ in response to 10 µM $CaCl_2$ were repeated in the presence of the PTP inhibitor cyclosporin A (CsA). PiC-depleted mitochondria still exhibited a greater depolarization in the presence of CsA (Fig. 3C). We further compared the ability for the PTP to open in KD *vs*. Ctrl preparations by evaluating the Ca^{2+} retention capacity (CRC) in response to 1 µM $CaCl_2$ pulses. PTP opening could not be provoked in the conditions used for Ca^{2+} and $\Delta\Psi_m$ measurements (Fig. 3D), likely because of the inclusion of adenine nucleotides (ATP-Mg^{2+}) in the incubation medium which would decrease PTP open probability (for review: (Giorgio, Guo et al., 2018)). Mitochondria incubated in medium devoid of ATP-Mg^{2+} and exposed to 10 µM $CaCl_2$ pulses robustly underwent PTP activation, evidenced by an abrupt and substantial depolarization (Fig. 3E). Fewer pulses were needed for PTP opening in Ctrl compared to PiC-depleted mitochondria (Fig. 3E). PTP opening could be inhibited by CsA, and the extent of the inhibition was similar in Ctrl and PiC-depleted mitochondria (Fig. 3E). We noted that protein expression of cyclophilin D (CypD), which increases PTP open probability, was elevated in KD muscle (evaluated in muscle lysates) (Suppl. Fig. 2). Altogether, this analysis of PTP opening indicates that PiC-depleted mitochondria *in situ* might be expected to be more resistant to PTP activation, even despite the elevated CypD expression, but that PTP opening is unlikely to occur in the conditions used to measure Ca^{2+} and $\Delta\Psi_m$. In summary, neither PTP opening nor Ca^{2+} stimulation of oxphos explains the greater depolarization of PiC-depleted mitochondria.

Higher protein levels of mtCU components in PiC-depleted mitochondria

Since PiC KD mitochondria exhibited greater RuR-inhibitable Ca^{2+} uptake, we questioned whether PiC-depleted mitochondria had a greater mtCU capacity. To investigate this, protein levels of the mtCU components were evaluated in the mitochondrial preparations used for the Ca^{2+} studies. Immunoblotting revealed that protein expression of MCU, EMRE and MICU1 were elevated by ~50% in KD mitochondria when compared to aconitase (ACO2), and also to TOM20 (Fig. 4A). That the increase in expression of each mtCU component was similar in PiC-depleted mitochondria suggested a greater abundance of the functional mtCU complex. To better evaluate if expression of the mtCU complex was increased, we determined the abundance of the native complex. To this end, samples of mitochondria were electrophoresed under non-denaturing conditions, then a

second-dimension gel was run under denaturing conditions and probed with antibodies against MCU and EMRE. MCU and EMRE immunoreactive bands corresponded to complexes of ~750 kDa and ~1000 kDa molecular weight (MW), and were detected in both Ctrl and KD samples, though at higher abundance in KD mitochondria (Suppl Fig. 3B, C). This experiment was repeated in a second pair on Ctrl and KD mitochondria, and had a similar outcome (not shown). Note that the Coomassie-stained gel (Suppl. Fig. 3A), and also the Complex II subunit SDHA (Suppl. Fig. 3D), serve as loading controls. An MCU-immunoreactive complex of ~1100 kDa was detected in cortical neurons (which also abundantly express MICU1 and MICU3) (Konig, Troder et al., 2016), and an ~750-800 kDa complex immunoreactive for MCU was detected in heart mitochondria (Lambert, Luongo et al., 2019) which expresses relatively low amounts of MICU1 (Antony, Paillard et al., 2016). Low EMRE expression can lead to the accumulation of lower MW MCU-immunoreactive mtCU intermediates (Konig et al., 2016). To determine if such an intermediate can be detected with our approach, and, thus, to demonstrate that an mtCU intermediate was detectable, we repeated the same electrophoresis protocols using skeletal muscle mitochondria from mice depleted of MICU1 in striated muscle (Debattisti et al., 2019) and floxed control mice. This model of skeletal muscle depletion of MICU1 shows substantial loss of EMRE protein and some loss of MCU protein (Debattisti et al., 2019). Electrophoresis under native followed by denaturing conditions resulted in only an MCU immunoreative band corresponding to a ~480 kDa complex in MICU1-depleted mitochondria but were no MCU immunoreactive bands corresponding to higher MW complexes (Suppl. Fig. 3E). In contrast, the control sample showed similar immunoreative bands corresponding to higher MW complexes (Suppl. Fig. 3E) as observed in PiC KD and Ctrl mitochondria (Suppl. Fig. 3B). Substantial loss of EMRE is also evident in the MICU1-depleted sample (Suppl. Fig. 3F) whereas EMRE is present in the Ctrl sample (Suppl. Fig. 3F). The appearance of the MCU-immunoreactive band associated with a lower MW complex in MICU1-depleted samples is similar to what was observed in HeLa cells lacking MICU1 and EMRE (Konig et al., 2016). Overall this analysis is consist with a greater abundance not only of components of mtCU in PiC KD mitochondria but of the assembled mtCU complex.

To evaluate MCU abundance at the level of the whole muscle (as a surrogate for mtCU capacity at the whole muscle level), immunoblotting was repeated in quadriceps lysates, with α-tubulin as the loading control. For comparison, mitochondrial proteins from the outer mitochondrial membrane (TOM20), and matrix (ACO2 and TFAM) were also we detected. All mitochondrial proteins were increased in KD quadriceps, suggesting a generalized increase in the abundance of mitochondria (Fig. 4B). We noted that, compared to the other mitochondrial proteins, the increase in MCU in KD quadriceps was ~2x higher. In summary, these data suggest that isolated KD mitochondria have a ~50% greater mtCU capacity, and that mtCU capacity may be even more expanded (~2x) at the

level of the whole muscle.

PiC depletion impairs Ca^{2+} handling during tetanic stimulation of skeletal muscle

The above results demonstrate that skeletal muscle mitochondria that are substantially depleted of the PiC not only robustly take up Ca^{2+} but do so to a greater extent than Ctrl mitochondria, and this occurs in conjunction with an increased mtCU capacity. Considering the ability of skeletal muscle mitochondria to buffer Ca^{2+} released from the sarcoplasmic reticulum (SR) (Boncompagni, Rossi et al., 2009, Shkryl & Shirokova, 2006), we evaluated the impact of PiC depletion on cytoplasmic Ca^{2+} transients. This was done in flexus digitorum brevis (FDB) fibers during single twitch (ST) or repeated tetanic stimulation (RTS), performed sequentially in each FDB preparation. Baseline $[Ca^{2+}]_c$ before each stimulus paradigm was similar between KD and Ctrl fibers (Fig. 5A). The ST stimulation evoked a similar ~50 nM cytoplasmic Ca^{2+} transient in fibers from both genotypes (Fig. 5A, B), that decayed with a similar kinetic (Suppl. Fig. 4). When the RTS protocol was tested, Ctrl fibers responded with a rapid-onset, substantial and sustained rise in $[Ca^{2+}]$c. $[Ca^{2+}]$c continued to increase throughout the stimulation period, though with a slower kinetic (Fig. 5A, C). Fibers depleted of PiC responded with the same pattern of cytoplasmic Ca^{2+} elevation, but with two differences. First, the rising phase tended to be faster in KD fibers (Fig. 5A). Second, the amplitude of the $[Ca^{2+}]$c rise was less in KD fibers, at both the onset and the end of the stimulation period (Fig. 5A); the maximal rise in $[Ca^{2+}]$c was significantly lower, by ~30% (Fig. 5C).

To gain insight into the lower amplitude response to RTS in KD fibers, protein levels of ER Ca^{2+} handling proteins were evaluated by immunoblotting in lysates from quadriceps muscle. KD and Ctrl muscle showed similar protein expression of the type 1 ryanodine receptor (RyR1) Ca^{2+} release channel, and the Ca^{2+}-binding proteins calsequestrin (CASQ1) and calreticulin (CALR) (Fig. 5D). Expression of the main SR Ca^{2+} uptake protein in skeletal muscle, SERCA1, was slightly (~20%) but significantly decreased in KD muscle, as was the protein level of the major skeletal muscle subunit of the L-type Ca^{2+} channel (CAV1.1) (Fig. 5D). These protein expression data indicate that the lower $[Ca^{2+}]$c response to RTS in KD fibers cannot be explained by changes in the abundance of ER Ca^{2+} release channels. Furthermore, the similar decay kinetic in KD and Ctrl fibers following RTS suggests that the small decrease in SERCA1 expression was unlikely of functional relevance.

PiC depletion leads to changes in the kinetics of muscle force generation

Finally, given the role of cytoplasmic Ca^{2+} in cross-bridge cycling and the suppressed cytoplasmic Ca^{2+} response to RTS in PiC-depleted muscle, we tested skeletal muscle force generation *ex vivo* using extensor digitorum longus (EDL) muscle challenged with ST and RTS stimulation. We first note that muscle cross-sectional area did not differ between Ctrl and KD EDL (Fig. 6A), consistent with the similar quadriceps weight in both genotypes (Fig. 1B). With ST stimulation, CSA-normalized force generated by PiC-depleted EDL trended lower (Fig. 6B), with no change in the rate of force

development (Fig. 6C), though time-to-peak was slightly (~20%) but consistently faster (Fig. 6D). With the RTS protocol, there was again a tendency for lesser force generation by PiC-depleted EDL (Fig. 6E), and, again, with no difference in the rate of force development (Fig. 6F). However, the time-to-peak was significantly and substantially delayed, by a factor of ~2, in PiC-depleted EDL (Fig. 6G); this is consistent with the lower $[Ca^{2+}]c$ rise in PiC-depleted EDL in response to a tetani (Fig. 5C).

Severe exercise intolerance in PiC KD mice coincides with greatly suppressed $[Ca^{2+}]c$ during a tetani

Though 3-week Tam-treated (13 week old) PiC-depleted mice were healthy, they were mildly exercise intolerant, evidenced by a ~25% decrease in running time on a treadmill and more frequent visits to the shock grid (Fig. 7A). In contrast, we noticed that, by 13-15 weeks after Tam treatment (22-24 weeks of age), exercise capacity deteriorated dramatically in PiC KD mice. Strikingly, these older KD mice were immobile on the shock grid after only ~5 minutes of treadmill running (Fig. 7B). Even after removal from the treadmill, KD mice remained immobile for several minutes and were also limp. This contrasts starkly with younger PiC-depleted mice that were mobile and behaved similarly to Ctrl mice immediately after running, and also with older Ctrl mice that had a similar running capacity and post-running behavior as younger Ctrl mice. We were therefore interested to determine if there was a progression in any aspect the Ca^{2+} phenotype in PiC KD mice. To this end, we repeated the RTS protocol in FDB fibers and immunoblot detection of Ca^{2+} handling proteins in muscle from older mice (13-15 weeks after Tam). In FDB fibers, resting $[Ca^{2+}]c$ was similar in Ctrl and KD preparations (Fig. 7C), and also similar to levels observed in younger mice. With RTS, the $[Ca^{2+}]c$ response in FDB from older Ctrl mice showed a pattern similar to that measured in younger Ctrl mice, though with a slightly elevated amplitude (Fig. 7C, compared to Fig. 5A,C). In contrast, PiC-depleted FDB from older mice responded to RTS with a $[Ca^{2+}]c$ rise that was slower in onset compared to the Ctrl response, and with a ~70% lower amplitude (Fig. 7C). Immunoblotting of muscle lysates showed a continued higher expression of all mtCU components in KD muscle from older mice, at levels similar to younger KD mice, along with unchanged levels of ER Ca^{2+} binding proteins, SERCA1 and Cav1.1 relative to Ctrl levels. However, muscle from older KD mice showed a substantial decrease in RyR1 protein expression, by ~50% (Fig. 7D), consistent with the dramatically suppressed $[Ca^{2+}]c$ rise during RTS in muscle from 22-24 week-old PiC KD mice.

DISCUSSION

MATERIALS and METHODS

Mouse model. Mice were used following mandated guidelines and protocols of care and use, approved by the Thomas Jefferson University Institutional Animal Care and Use Committee

(IACUC). Mice were maintained at 22 °C under a standard 12-hour light/12-hour dark cycle. Only male mice were used for experiments. Mice with specific PiC-loss in the skeletal muscle were generated by crossing mice with floxed PiC alleles (Kwong et al., 2014) with mice expressing human skeletal α-actin promoter driving Cre recombinase, which is induced by tamoxifen (Tam) (HSA-MCM (McCarthy et al., 2012). Both models were on the C57BL/6 background. Control ($PiC^{fl/fl}$) and PiC KD ($Cre+PiC^{fl/fl}$) were injected intraperitoneally with Tam (25 mg/kg/mouse, i.p.) for 4 consecutive days starting when mice were 9 weeks old. Mice were sacrificed 3 and 12 weeks after the final Tam injection.

Isolation of skeletal muscle mitochondria. Skeletal muscle mitochondria were isolated as described in (Seifert, Bezaire et al., 2008). All steps were performed at 4°C or on ice. Skeletal muscle from mouse forelimb and hindlimb was dissected and placed in basic medium (BM) containing 140 mM KCl, 20 mM HEPES, 5 mM $MgCl_2$, 1 mM EGTA, pH 7.0. Muscle was cleaned of fat and connective tissue, minced and placed in 30 mL of homogenization medium (HM) composed of BM with the following additions: 1 mM Mg^{2+}-ATP, 2 mM EGTA and 1% fatty acid free BSA (w/v) containing two units of protease from Bacillus licheniformis (Sigma, P5380) per muscle weight (g). The tissue was homogenized using a glass Potter-Elvehjem homogenizer with a Teflon pestle (15 passes at 500 r.p.m). The tissue suspension was centrifuged at 2,000 r.p.m. for 10 min, then supernatant was collected and centrifuged at 9,000 r.p.m. for 8 min. The resulting pellet was resuspended and incubated in BM for 5 min. Then, samples were centrifuged at 2,000 r.p.m. for 10 min, the supernatant was filtered through a 70 μM cell strainer (Falcon, 352250) then spun at 9,000 r.p.m. The final pellet was resuspended in BM (to have protein concentration ~25 mg/ml). Protein concentration was determined by BCA assay (ThermoFisher Scientific, 23225).

Fluorometric measurements in suspensions of isolated mitochondria (PTI). For fluorometric measurements, skeletal muscle mitochondria were depleted of endogenous phosphate. To achieve this, mitochondria pellet was resuspended in BM with the following additions: 0.75U/mL hexokinase (Roche, 11426362001), 1 mM glucose, 0.5 mM ADP, 1 mM $MgCl_2$, 5 mM malate and 5 mM pyruvate, and then incubated for 10 min at 35 °C. After that, the sample was centrifuged at 9,000 *g* for 10 min, and the pellet obtained was resuspended in BM. For fluorometric measurements of mitochondrial matrix Ca^{2+} concentration ($[Ca^{2+}]_m$), skeletal muscle mitochondria suspension was incubated with 20 μM Fura-FF, AM (AAT Bioquest, 21027) and 0.3 % pluronic acid (Invitrogen, P6867) at 35 °C for 30 min. After that, the suspension was centrifuged at 9,000 *g* for 10 min at 4 °C and the pellet obtained was resuspended in BM. All fluorometric measurements were performed

using a running buffer (RB) composed of an intracellular medium (ICM) containing 120 mM KCl, 10 mM NaCl, 1mM KH_2PO_4, 20 mM Tris-HEPES, pH 7.2, supplemented with protease inhibitors (1 µg/mL each of leupeptin, pepstatin and antipain), 2 µM thapsigargin, 2 mM Mg-ATP, 0.5 µL/mL of 1 M KOH and 1 mM of each pyruvate and malate or 10 mM succinate + 1µM rotenone. The extramitochondrial Ca^{2+} concentration ($[Ca^{2+}]_c$), was assessed using Rhod-FF, tripotassium salt (AAT Bioquest, 21076) or 1 µM Fura-lowAff, (AAT Bioquest, 21028). Mitochondrial membrane potential ($\Delta\Psi_m$) was measured with TMRM (Invitrogen, T668). Fluorescence was monitored with a multiwavelength excitation/dual wavelength emission fluorimeter (DeltaRAM, Photon Technology International). After the addition of $CaCl_2$ pulses, 6.7 µM FCCP was added to dissipate the $\Delta\Psi_m$, followed by an addition of 4 µM ionomycin. Calibration of the $[Ca^{2+}]$ signal was carried out at the end of each measurement, adding 1 mM $CaCl_2$, followed by 10 mM EGTA/Tris, pH 8.5.

Bioenergetics analyses in isolated skeletal mitochondria. O_2 consumption (JO_2) was measured using the Seahorse XF24 Analyzer (Seahorse Bioscience, Billerica, MA, USA). Isolated mitochondria were studied as described (Moffat, Bhatia et al., 2014, Vasquez-Trincado, Patel et al., 2021). Each well of the custom microplate contained 10 µg of mitochondria suspended in mitochondria assay medium (MAS): 70 mM sucrose, 22 mM mannitol, 10 mM KH_2PO_4, 5 mM $MgCl_2$, 2 mM HEPES, 1 mM EGTA, 0.2% fatty acid free BSA, pH 7.4 at 37°C. The amount of mitochondria used was optimized to obtain a linear O_2 *vs*. time signal under all conditions. The microplate was centrifuged at 2,000 *g* for 20 min at 4°C. Mitochondria were energized using malate-pyruvate (5 mM/10 mM). Maximal oxidative phosphorylation was measured using saturating [ADP] (2.8 mM). Maximal leak JO_2 was measured in the presence of the ATP synthase inhibitor oligomycin (4 µg/mL). Maximal uncoupled JO_2 was measured using the chemical uncoupler FCCP (6.7 µM).

Immunoblot analysis. For western blot analysis, skeletal muscle tissue was rapidly frozen in liquid nitrogen. Tissue was homogenized on ice in a lysis buffer containing: 150 mM NaCl, 25 mM HEPES, 2.5 mM EGTA, 1% Triton 100X, 1% Igepal (10%), 0.10% SDS, 0.1% Deoxycholate, 10% Glycerol, protease inhibitor (Roche 11873580001) and phosphatase inhibitor cocktail (200 mM sodium fluoride, 200 mM, imidazole, 115 mM sodium molybdate, 200 mM sodium orthovanadate, 400 mM sodium tartrate dihydrate, 100 mM sodium pyrophosphate and 100 mM β-glycerophosphate), using a glass/Teflon homogenizer at 500 rpm. Muscle lysates were then incubated at 4°C for 45 min, then centrifuged at 18,000 *g* for 20 min. Protein concentration was measured from the supernatant with BCA assay. For western blot analysis from isolated mitochondria, lysis was obtained using RIPA buffer (Sigma-Aldrich R0278) containing protease and phosphatase inhibitors. Samples were

incubated on ice for 30 min and vortexed every 5-10 min, and then lysates were centrifugated at 12,000 r.p.m. for 10 min. From the supernatant, protein concentration was measured by BCA assay. Primary antibodies were used for overnight incubation ,diluted in TBS-T 1% (20 mM Tris, 0.9 % NaCl, 0.1 % Tween 20, pH 7.4), and are listed below.

Primary Antibodies used in immunoblot analysis

Antibody	Catalog Number	Dilution	Host
SLC25A3/PiC	Custom made	1:1000	Rabbit
α-Tubulin	CST-2215S	1:1000	Rabbit
Cyclophilin D	Abcam (Ab)-110334	1:10000	Mouse
MCU	HPA016480 (Sigma-Aldrich)	1:1000	Rabbit
TOM20	ProteinTech 11802	1:1000	Rabbit
Aconitase 2	Ab-129069	1:1000	Rabbit
mtTFA/TFAM	Santa Cruz (SC)-23588	1:500	Mouse
EMRE	Bethyl A300BL19208	1:1000	Rabbit
MICU1	HPA037479	1:500	Rabbit
SERCA1	Custom made, YenZym	1:1000	Rabbit
Calsequestrin	Ab-3516	1:1000	Rabbit
Calreticulin	Cell Signaling Technology (CST)-2891	1:1000	Rabbit
RYR1	Developmental Studies Hybridoma Bank (DHSB)-34C	1:100	Mouse
GRB2	SC-8034	1:1000	Rabbit
Vinculin	CST-13901	1:1000	Rabbit

Blue native and second dimension electrophoresis. After BCA, 100ug of isolated skeletal muscle mitochondria were extracted with 4% digitonin (D141-100MG,Sigma) in extraction buffer (30mM HEPES, 12% glycerol, 150mM potassium acetate, 2mM aminocaproic acid, 2mM EDTA disodium salt, protease inhibitor tablet, pH 7.4). To the supernatant was added 1ul of 1:400 diluted G-250: extraction buffer and the samples were loaded on a NativePAGE™ NovexR 3–12% Bis-Tris gel. The gel was ran overnight (on ice, 30V) in 1x NativePAGE™ Running buffer (as anode buffer) and 1x dark blue cathode buffer for 1h then switched to 1x light blue cathode buffer for the rest of the run. Each sample was run in duplicate; one of the lanes was Commassie blue stained and the second lane was run on a second dimension SDS gel. The lane for the second dimension was excised, then equilibrated in a Equilibration (Eq) buffer containing 50 mM Tris, 6 M Urea, 30% glycerol, 2% SDS, pH 8.5, for 5min, then switched to Eq. buffer + 200mM DTT for 30 min, followed by Eq. buffer + 135mM iodoacetamide for 15 min and 2x Eq. buffer for 15min incubation. The lane was then inserted into NuPAGE™ 4-12% Bis-Tris Gel with 2D well and run in 1x MOPS running buffer. The gel was transferred to 0.2um nitrocellulose membrane and used for protein detection.

FDB fiber isolation and culture. Mouse flexus digitorum brevis (FDB) isolation was performed

following general guidelines described in (Debattisti et al., 2019, Eisner, Lenaers et al., 2014). Briefly, FDB muscles from each footpad were quickly dissected and digested with 3 mg/mL of collagenase type 2 (Worthington Biochemical Corporation, LS004194) at 37 °C for 1-2 hrs. under agitation. The collagenase solution was prepared in DMEM/F12 medium (Lonza, BE04-687F/U1) without serum. After incubation with collagenase, FDB fibers were incubated with DMEM/F12 + 10% horse serum (Gibco, 16050130) containing 2 mM glutamine, 100 U/ml penicillin and 100mg/ml streptomycin (ThermoFisher Scientific 10378016). Mechanical disaggregation of the muscle was carefully done using glass pipettes, until individual fibers were obtained, which were plated on glass bottom microwell dishes (MatTek Corporation, 801002) that had been pre-treated with Cell-Tak (Corning, 354240). Fibers were allowed to attach to the plate in an incubator at 37°C with 5% CO_2-humidified air for 2-3 hrs. prior to cell imaging.

Live fiber imaging. Imaging measurements were done using a 2% BSA-extracellular medium (ECM) containing: 121 mM NaCl, 5 mM NaHCO3, 4.7 mM KCl, 1.2 mM KH2PO4, 1.2 mM MgSO4, 2 mM CaCl2, 10 mM glucose and 10 mM Na-HEPES, pH 7.4, at 35 °C. For [Ca2+]c imaging, fibers were loaded with 2 μM Fura-2, AM (Invitrogen, F-1221) at room temperature in 2% BSA-ECM in presence of 0.003% pluronic acid (Invitrogen, P6867) and 100 μM sulfinpyrazone (Sigma, 9509), for 20 min. After calcium dye loading, fibers were carefully rinsed with ECM, and maintained in ECM containing 75 μM BTS (Tocris, 1870) and 100 μM sulfinpyrazone at 35 °C. Images were acquired using an ImagEM EM-CCD camera (Hamamatsu) fitted to an Olympus IX81 microscope with LED source (Lambda TLED+, Sutter Instruments). Detection of Fura-2 fluorescence was recorded using excitation 340/380 nm (emission 540/50 nm). Calibration of the Fura2-AM signal was carried out by adding 1 mM $CaCl_2$, followed by 10 mM EGTA/Tris, pH 8.5.

Electrical stimulation. FDB fibers were electrically stimulated by means of field stimulation as described (Eisner et al., 2014). The repetitive tetanic stimulation (RTS) protocol was: 100 tetani, 100 Hz, for 500 ms every 2.5 s, pulse length 2 ms, at 2 V. For single twitch (ST), fibers were stimulated at 1 Hz every 60 s, pulse length 2 ms at 2V. For the electrical stimulation, a perfusion chamber was used (Warner Instruments, RC-37FS, 64-0366) holding two parallel platinum electrodes positioned 6 mm apart. The chamber was connected to a pulse stimulator (Aurora Scientific Inc, 701C) and an oscilloscope (Tektronix, TDS 220). The RTS and ST frequency was controlled by an Optogenetics TTL pulse generator (Doric, OPTG4).

Ex vivo physiology in EDL. Evaluation of *ex vivo* EDL force was performed as described (Loro,

Seifert et al., 2015, Yang, Loro et al., 2020) using an Aurora Mouse 1200A System equipped with Dynamic Muscle Control v.5.415 software. Briefly, EDL muscles were dissected and maintained in constantly oxygenated Ringer's solution (100 mM NaCl, 4.7 mM KCl, 3.4 mM CaCl2, 1.2 mM KH2PO4, 1.2 mM MgSO4, 25 mM HEPES, 5.5 mM D-glucose) at 24 °C. The twitch stimulation protocol applied was a single 30-V stimulus with a duration of 0.2 ms. For measuring tetanic maximal force generation, the 30-V stimulus lasting 0.2 ms was repeated at a frequency of 120 Hz for 500 ms. Five minutes were allowed between two tetanic contractions to ensure muscle recovery.

Quantification and statistical analysis. Averaged data are presented as the mean ± standard error of the mean (sem). Data analysis was performed using GraphPad Prism 8.2.1 Software. Paired Student's *t* test for comparison of two means and one or two-way analysis of variance followed by Tukey post-hoc comparisons, for multiple comparisons, were performed as appropriate. P value < 0.05 was considered significant. For details are provided in Results and the figure legends.

FIGURE LEGENDS and FIGURE can be found after the REFERENCES

REFERENCES

Antony AN, Paillard M, Moffat C, Juskeviciute E, Correnti J, Bolon B, Rubin E, Csordas G, Seifert EL, Hoek JB, Hajnoczky G (2016) MICU1 regulation of mitochondrial Ca(2+) uptake dictates survival and tissue regeneration. *Nat Commun* 7: 10955

Basso E, Petronilli V, Forte MA, Bernardi P (2008) Phosphate is essential for inhibition of the mitochondrial permeability transition pore by cyclosporin A and by cyclophilin D ablation. *J Biol Chem* 283: 26307-11

Baughman JM, Perocchi F, Girgis HS, Plovanich M, Belcher-Timme CA, Sancak Y, Bao XR, Strittmatter L, Goldberger O, Bogorad RL, Koteliansky V, Mootha VK (2011) Integrative genomics identifies MCU as an essential component of the mitochondrial calcium uniporter. *Nature* 476: 341-5

Boncompagni S, Rossi AE, Micaroni M, Beznoussenko GV, Polishchuk RS, Dirksen RT, Protasi F (2009) Mitochondria are linked to calcium stores in striated muscle by developmentally regulated tethering structures. *Mol Biol Cell* 20: 1058-67

Chalmers S, Nicholls DG (2003) The relationship between free and total calcium concentrations in the matrix of liver and brain mitochondria. *J Biol Chem* 278: 19062-70

Crompton M, Costi A (1988) Kinetic evidence for a heart mitochondrial pore activated by Ca2+, inorganic phosphate and oxidative stress. A potential mechanism for mitochondrial dysfunction during cellular Ca2+ overload. *Eur J Biochem* 178: 489-501

Csordas G, Golenar T, Seifert EL, Kamer KJ, Sancak Y, Perocchi F, Moffat C, Weaver D, Perez SF, Bogorad R, Koteliansky V, Adijanto J, Mootha VK, Hajnoczky G (2013) MICU1 controls both the threshold and cooperative activation of the mitochondrial Ca(2)(+) uniporter. *Cell Metab* 17: 976-987

De Stefani D, Raffaello A, Teardo E, Szabo I, Rizzuto R (2011) A forty-kilodalton protein of the inner membrane is the mitochondrial calcium uniporter. *Nature* 476: 336-40

Debattisti V, Horn A, Singh R, Seifert EL, Hogarth MW, Mazala DA, Huang KT, Horvath R, Jaiswal JK, Hajnoczky G (2019) Dysregulation of Mitochondrial Ca(2+) Uptake and Sarcolemma Repair Underlie Muscle Weakness and Wasting in Patients and Mice Lacking MICU1. *Cell Rep* 29: 1274-1286 e6

Dogan SA, Cerutti R, Beninca C, Brea-Calvo G, Jacobs HT, Zeviani M, Szibor M, Viscomi C (2018) Perturbed Redox Signaling Exacerbates a Mitochondrial Myopathy. *Cell Metab* 28: 764-775 e5

Eisner V, Csordas G, Hajnoczky G (2013) Interactions between sarco-endoplasmic reticulum and mitochondria in cardiac and skeletal muscle - pivotal roles in Ca(2)(+) and reactive oxygen species signaling. *J Cell Sci* 126: 2965-78

Eisner V, Lenaers G, Hajnoczky G (2014) Mitochondrial fusion is frequent in skeletal muscle and supports excitation-contraction coupling. *J Cell Biol* 205: 179-95

Favaro G, Romanello V, Varanita T, Andrea Desbats M, Morbidoni V, Tezze C, Albiero M, Canato M, Gherardi G, De Stefani D, Mammucari C, Blaauw B, Boncompagni S, Protasi F, Reggiani C, Scorrano L, Salviati L, Sandri M (2019) DRP1-mediated mitochondrial shape controls calcium homeostasis and muscle mass. *Nat Commun* 10: 2576

Fieni F, Lee SB, Jan YN, Kirichok Y (2012) Activity of the mitochondrial calcium uniporter varies greatly between tissues. *Nat Commun* 3: 1317

Gherardi G, Nogara L, Ciciliot S, Fadini GP, Blaauw B, Braghetta P, Bonaldo P, De Stefani D, Rizzuto R, Mammucari C (2019) Loss of mitochondrial calcium uniporter rewires skeletal muscle metabolism and substrate preference. *Cell Death Differ* 26: 362-381

Giorgio V, Guo L, Bassot C, Petronilli V, Bernardi P (2018) Calcium and regulation of the mitochondrial permeability transition. *Cell Calcium* 70: 56-63

Glancy B, Balaban RS (2012) Role of mitochondrial Ca2+ in the regulation of cellular energetics. *Biochemistry* 51: 2959-73

Havlickova Karbanova V, Cizkova Vrbacka A, Hejzlarova K, Nuskova H, Stranecky V, Potocka A, Kmoch S, Houstek J (2012) Compensatory upregulation of respiratory chain complexes III and IV in isolated deficiency of ATP synthase due to TMEM70 mutation. *Biochim Biophys Acta* 1817: 1037-43

Joseph AM, Rungi AA, Robinson BH, Hood DA (2004) Compensatory responses of protein import and transcription factor expression in mitochondrial DNA defects. *Am J Physiol Cell Physiol* 286: C867-75

Konig T, Troder SE, Bakka K, Korwitz A, Richter-Dennerlein R, Lampe PA, Patron M, Muhlmeister M, Guerrero-Castillo S, Brandt U, Decker T, Lauria I, Paggio A, Rizzuto R, Rugarli EI, De Stefani D, Langer T (2016) The m-AAA Protease Associated with Neurodegeneration Limits MCU Activity in Mitochondria. *Mol Cell* 64: 148-162

Kovarova N, Cizkova Vrbacka A, Pecina P, Stranecky V, Pronicka E, Kmoch S, Houstek J (2012) Adaptation of respiratory chain biogenesis to cytochrome c oxidase deficiency caused by SURF1 gene mutations. *Biochim Biophys Acta* 1822: 1114-24

Kwong JQ, Davis J, Baines CP, Sargent MA, Karch J, Wang X, Huang T, Molkentin JD (2014) Genetic deletion of the mitochondrial phosphate carrier desensitizes the mitochondrial permeability transition pore and causes cardiomyopathy. *Cell Death Differ* 21: 1209-17

Kwong JQ, Huo J, Bround MJ, Boyer JG, Schwanekamp JA, Ghazal N, Maxwell JT, Jang YC, Khuchua Z, Shi K, Bers DM, Davis J, Molkentin JD (2018) The mitochondrial calcium uniporter underlies metabolic fuel preference in skeletal muscle. *JCI Insight* 3

Lambert JP, Luongo TS, Tomar D, Jadiya P, Gao E, Zhang X, Lucchese AM, Kolmetzky DW, Shah NS, Elrod JW (2019) MCUB Regulates the Molecular Composition of the Mitochondrial Calcium Uniporter Channel to Limit Mitochondrial Calcium Overload During Stress. *Circulation* 140: 1720-1733

Lehninger AL (1974) Role of phosphate and other proton-donating anions in respiration-coupled transport of Ca2+ by mitochondria. *Proc Natl Acad Sci U S A* 71: 1520-4

Leung AW, Varanyuwatana P, Halestrap AP (2008) The mitochondrial phosphate carrier interacts with cyclophilin D and may play a key role in the permeability transition. *J Biol Chem* 283: 26312-23

Lewis-Smith D, Kamer KJ, Griffin H, Childs AM, Pysden K, Titov D, Duff J, Pyle A, Taylor RW, Yu-Wai-Man P, Ramesh V, Horvath R, Mootha VK, Chinnery PF (2016) Homozygous deletion in MICU1 presenting with fatigue and lethargy in childhood. *Neurol Genet* 2: e59

Logan CV, Szabadkai G, Sharpe JA, Parry DA, Torelli S, Childs AM, Kriek M, Phadke R, Johnson CA, Roberts NY, Bonthron DT, Pysden KA, Whyte T, Munteanu I, Foley AR, Wheway G, Szymanska K, Natarajan S, Abdelhamed ZA, Morgan JE et al. (2014) Loss-of-function mutations in MICU1 cause a brain and muscle disorder linked to primary alterations in mitochondrial calcium signaling. *Nat Genet* 46: 188-93

Loro E, Seifert EL, Moffat C, Romero F, Mishra MK, Sun Z, Krajacic P, Anokye-Danso F, Summer RS, Ahima RS, Khurana TS (2015) IL-15Ralpha is a determinant of muscle fuel utilization, and its loss protects against obesity. *Am J Physiol Regul Integr Comp Physiol* 309: R835-44

Mallilankaraman K, Cardenas C, Doonan PJ, Chandramoorthy HC, Irrinki KM, Golenar T, Csordas G, Madireddi P, Yang J, Muller M, Miller R, Kolesar JE, Molgo J, Kaufman B, Hajnoczky G, Foskett JK, Madesh M (2012) MCUR1 is an essential component of mitochondrial Ca2+ uptake that regulates cellular metabolism. *Nat Cell Biol* 14: 1336-43

Mammucari C, Gherardi G, Zamparo I, Raffaello A, Boncompagni S, Chemello F, Cagnin S, Braga A, Zanin S, Pallafacchina G, Zentilin L, Sandri M, De Stefani D, Protasi F, Lanfranchi G, Rizzuto R (2015) The mitochondrial calcium uniporter controls skeletal muscle trophism in vivo. *Cell Rep* 10: 1269-79

Mayr JA, Merkel O, Kohlwein SD, Gebhardt BR, Bohles H, Fotschl U, Koch J, Jaksch M, Lochmuller H, Horvath R, Freisinger P, Sperl W (2007) Mitochondrial phosphate-carrier deficiency: a novel disorder of oxidative phosphorylation. *Am J Hum Genet* 80: 478-84

Mayr JA, Zimmermann FA, Horvath R, Schneider HC, Schoser B, Holinski-Feder E, Czermin B, Freisinger P, Sperl W (2011) Deficiency of the mitochondrial phosphate carrier presenting as myopathy and cardiomyopathy in a family with three affected children. *Neuromuscul Disord* 21: 803-8

McCarthy JJ, Srikuea R, Kirby TJ, Peterson CA, Esser KA (2012) Inducible Cre transgenic mouse strain for skeletal muscle-specific gene targeting. *Skelet Muscle* 2: 8

McCormack JG, Halestrap AP, Denton RM (1990) Role of calcium ions in regulation of mammalian intramitochondrial metabolism. *Physiol Rev* 70: 391-425

Modesti L, Danese A, Angela Maria Vitto V, Ramaccini D, Aguiari G, Gafa R, Lanza G, Giorgi C, Pinton P (2021) Mitochondrial Ca(2+) Signaling in Health, Disease and Therapy. *Cells* 10

Moffat C, Bhatia L, Nguyen T, Lynch P, Wang M, Wang D, Ilkayeva OR, Han X, Hirschey MD, Claypool SM, Seifert EL (2014) Acyl-CoA thioesterase-2 facilitates mitochondrial fatty acid oxidation in the liver. *J Lipid Res* 55: 2458-70

Musa S, Eyaid W, Kamer K, Ali R, Al-Mureikhi M, Shahbeck N, Al Mesaifri F, Makhseed N, Mohamed Z, AlShehhi WA, Mootha VK, Juusola J, Ben-Omran T (2019) A Middle Eastern Founder Mutation Expands the Genotypic and Phenotypic Spectrum of Mitochondrial MICU1 Deficiency: A Report of 13 Patients. *JIMD Rep* 43: 79-83

Nicholls DG (2005) Mitochondria and calcium signaling. *Cell Calcium* 38: 311-7

Paillard M, Csordas G, Huang KT, Varnai P, Joseph SK, Hajnoczky G (2018) MICU1 Interacts with the D-Ring of the MCU Pore to Control Its Ca(2+) Flux and Sensitivity to Ru360. *Mol Cell* 72: 778-785 e3

Pan X, Liu J, Nguyen T, Liu C, Sun J, Teng Y, Fergusson MM, Rovira, II, Allen M, Springer DA, Aponte AM, Gucek M, Balaban RS, Murphy E, Finkel T (2013) The physiological role of mitochondrial calcium revealed by mice lacking the mitochondrial calcium uniporter. *Nat Cell Biol* 15: 1464-72

Patron M, Raffaello A, Granatiero V, Tosatto A, Merli G, De Stefani D, Wright L, Pallafacchina G, Terrin A, Mammucari C, Rizzuto R (2013) The mitochondrial calcium uniporter (MCU): molecular identity and physiological roles. *J Biol Chem* 288: 10750-8

Pereira RO, Tadinada SM, Zasadny FM, Oliveira KJ, Pires KMP, Olvera A, Jeffers J, Souvenir R, McGlauflin R, Seei A, Funari T, Sesaki H, Potthoff MJ, Adams CM, Anderson EJ, Abel ED (2017) OPA1 deficiency promotes secretion of FGF21 from muscle that prevents obesity and insulin resistance. *EMBO J* 36: 2126-2145

Perocchi F, Gohil VM, Girgis HS, Bao XR, McCombs JE, Palmer AE, Mootha VK (2010) MICU1 encodes a mitochondrial EF hand protein required for Ca(2+) uptake. *Nature* 467: 291-6
Plovanich M, Bogorad RL, Sancak Y, Kamer KJ, Strittmatter L, Li AA, Girgis HS, Kuchimanchi S, De Groot J, Speciner L, Taneja N, Oshea J, Koteliansky V, Mootha VK (2013) MICU2, a paralog of MICU1, resides within the mitochondrial uniporter complex to regulate calcium handling. *PLoS One* 8: e55785
Raffaello A, De Stefani D, Sabbadin D, Teardo E, Merli G, Picard A, Checchetto V, Moro S, Szabo I, Rizzuto R (2013) The mitochondrial calcium uniporter is a multimer that can include a dominant-negative pore-forming subunit. *EMBO J* 32: 2362-76
Sancak Y, Markhard AL, Kitami T, Kovacs-Bogdan E, Kamer KJ, Udeshi ND, Carr SA, Chaudhuri D, Clapham DE, Li AA, Calvo SE, Goldberger O, Mootha VK (2013) EMRE is an essential component of the mitochondrial calcium uniporter complex. *Science* 342: 1379-82
Seifert EL, Bezaire V, Estey C, Harper ME (2008) Essential role for uncoupling protein-3 in mitochondrial adaptation to fasting but not in fatty acid oxidation or fatty acid anion export. *J Biol Chem* 283: 25124-31
Seifert EL, Ligeti E, Mayr JA, Sondheimer N, Hajnoczky G (2015) The mitochondrial phosphate carrier: Role in oxidative metabolism, calcium handling and mitochondrial disease. *Biochem Biophys Res Commun* 464: 369-75
Shamseldin HE, Alasmari A, Salih MA, Samman MM, Mian SA, Alshidi T, Ibrahim N, Hashem M, Faqeih E, Al-Mohanna F, Alkuraya FS (2017) A null mutation in MICU2 causes abnormal mitochondrial calcium homeostasis and a severe neurodevelopmental disorder. *Brain* 140: 2806-2813
Shkryl VM, Shirokova N (2006) Transfer and tunneling of Ca2+ from sarcoplasmic reticulum to mitochondria in skeletal muscle. *J Biol Chem* 281: 1547-54
Tezze C, Romanello V, Desbats MA, Fadini GP, Albiero M, Favaro G, Ciciliot S, Soriano ME, Morbidoni V, Cerqua C, Loefler S, Kern H, Franceschi C, Salvioli S, Conte M, Blaauw B, Zampieri S, Salviati L, Scorrano L, Sandri M (2017) Age-Associated Loss of OPA1 in Muscle Impacts Muscle Mass, Metabolic Homeostasis, Systemic Inflammation, and Epithelial Senescence. *Cell Metab* 25: 1374-1389 e6
Touvier T, De Palma C, Rigamonti E, Scagliola A, Incerti E, Mazelin L, Thomas JL, D'Antonio M, Politi L, Schaeffer L, Clementi E, Brunelli S (2015) Muscle-specific Drp1 overexpression impairs skeletal muscle growth via translational attenuation. *Cell Death Dis* 6: e1663
Varanyuwatana P, Halestrap AP (2012) The roles of phosphate and the phosphate carrier in the mitochondrial permeability transition pore. *Mitochondrion* 12: 120-5
Vasquez-Trincado C, Patel M, Sivaramakrishnan A, Bekeova C, Anderson-Pullinger L, Wang N, Tang HY, Seifert EL (2021) Adaptation of the heart to Frataxin depletion: Evidence that integrated stress response can predominate over mTORC1 activation. *Hum Mol Genet*
Viscomi C, Bottani E, Civiletto G, Cerutti R, Moggio M, Fagiolari G, Schon EA, Lamperti C, Zeviani M (2011) In vivo correction of COX deficiency by activation of the AMPK/PGC-1alpha axis. *Cell Metab* 14: 80-90
Wolf SG, Mutsafi Y, Dadosh T, Ilani T, Lansky Z, Horowitz B, Rubin S, Elbaum M, Fass D (2017) 3D visualization of mitochondrial solid-phase calcium stores in whole cells. *Elife* 6
Yang S, Loro E, Wada S, Kim B, Tseng WJ, Li K, Khurana TS, Arany Z (2020) Functional effects of muscle PGC-1alpha in aged animals. *Skelet Muscle* 10: 14

Figure 1

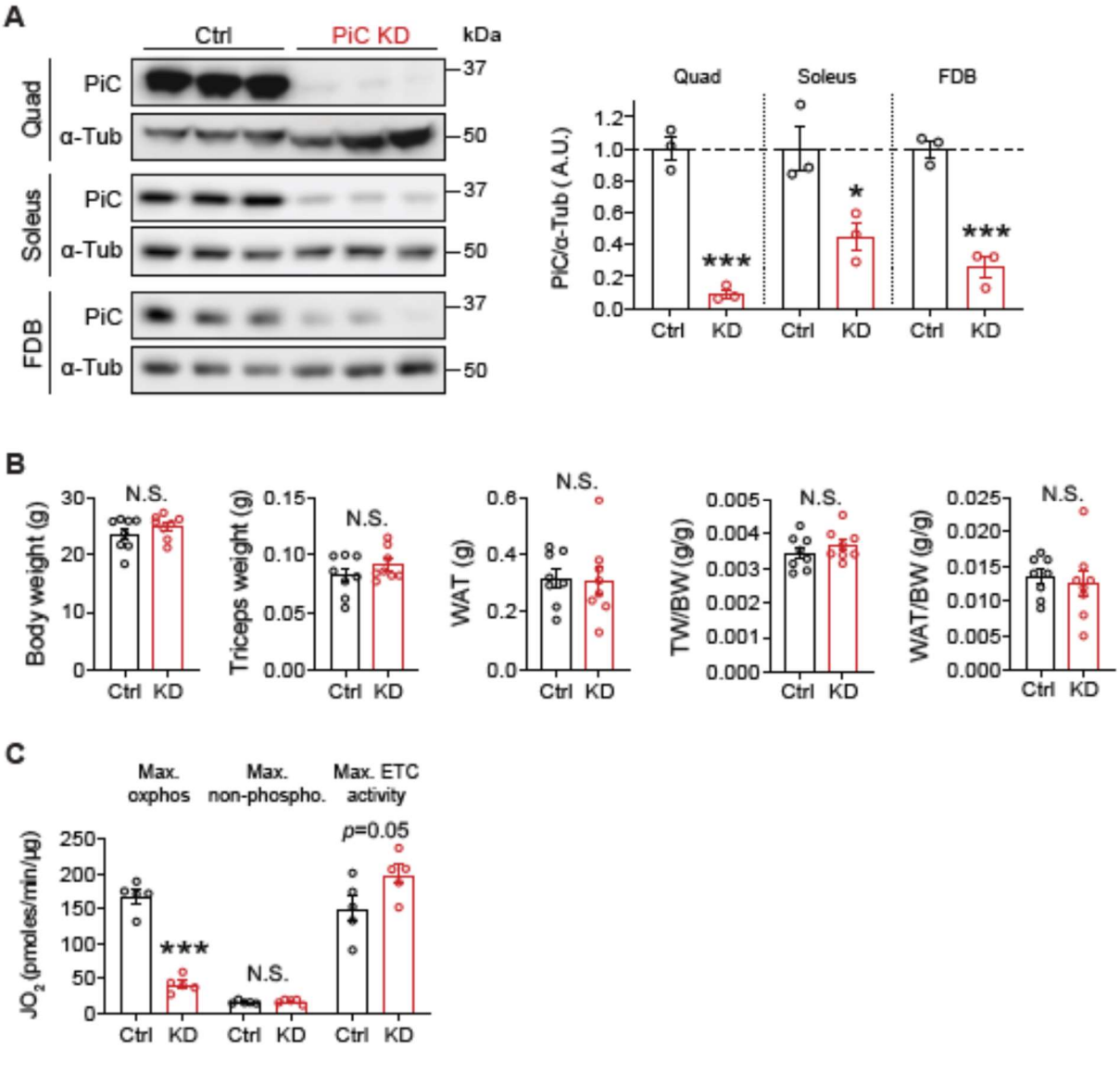
A
Ctrl
PiC KD
kDa
Quad
Soleus
FDB
PiC
α-Tub
37
50
Quad
Soleus
FDB
PiC/α-Tub (A.U.)
1.2
1.0
0.8
0.6
0.4
0.2
0.0
***
*
***
Ctrl
KD
B
Body weight (g)
Triceps weight (g)
WAT (g)
TW/BW (g/g)
WAT/BW (g/g)
N.S.
C
Max. oxphos
Max. non-phospho.
Max. ETC activity
p=0.05
JO2 (pmoles/min/µg)
250
200
150
100
50
0

Figure 1: New model of PiC depletion in skeletal muscle.

(A) Representative immunoblots of PiC and α-Tubulin (loading control) of lysates from quadriceps (Quad), soleus, and flexus digitorum longus (FDB), from Ctrl and PiC KD mice. *Right*: Averaged (± sem) values of PiC relative to α-Tubulin, (n = 3/genotype).

(B) Body weight, muscle weight and white adipose tissue (WAT) from Ctrl and PiC KD mice (n = 7/genotype).

(C) Oxygen consumption rate (JO_2) measured in isolated skeletal muscle mitochondria supplied with pyruvate/malate (P/M; 10 mM/5 mM). Max oxphos: JO_2 reflects maximal oxidative phosphorylation when saturating [ADP] and [substrate] were used. Max non-phosphorylating: JO_2 reflects maximal non-phosphorylating oxidation when oligomycin was used to inhibit the ATP synthase. Max ETC activity: JO_2 reflects the maximal electron transport chain (ETC) activity for the prevailing substrate when the chemical uncoupler, FCCP (1 µM) was used (n=5/genotype).

All bar charts: individual data points are shown, and bars represent mean ± s.e.m. Statistical comparison: unpaired t-test, *p<0.05, **p<0.01, ***p<0.01. N.S.: not significant.

Figure 2

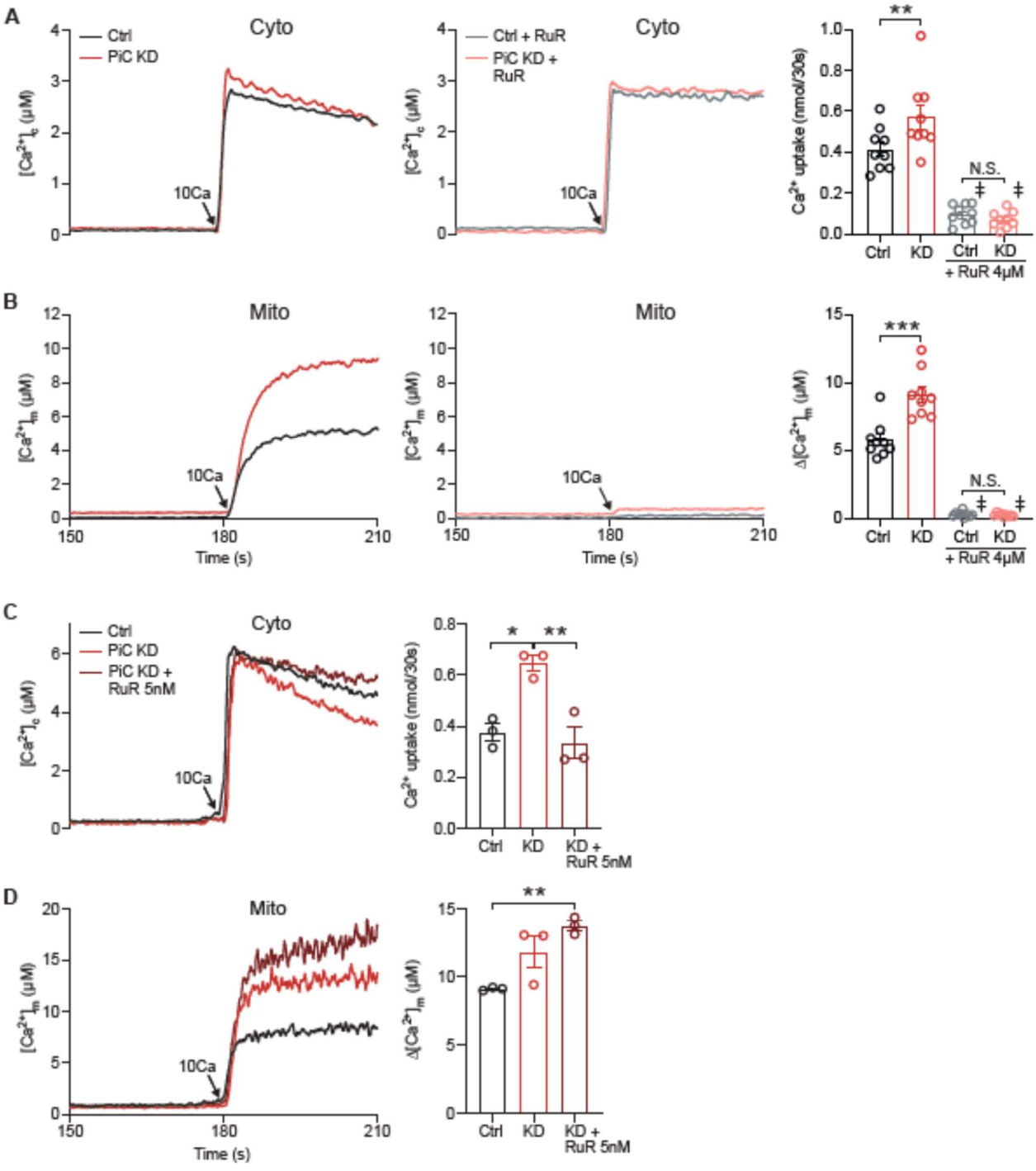
A
Cyto
Ctrl
PiC KD
10Ca
Ctrl + RuR
PiC KD + RuR
Ca2+ uptake (nmol/30s)
N.S.
Ctrl
KD
Ctrl + RuR 4μM
B
Mito
Time (s)
Δ[Ca2+]m (μM)
C
PiC KD + RuR 5nM
KD + RuR 5nM
D

Figure 2: PiC-depleted mitochondria display increased Ca^{2+} uptake rate and matrix free Ca^{2+} in response to $CaCl_2$ addition.

(A) Representative time course of the mitochondrial clearance of the $[Ca^{2+}]_c$ rise upon addition of a 10 µM $CaCl_2$ bolus (10Ca) in suspensions of Ctrl (black) and PiC KD (red) skeletal muscle mitochondria and in presence of RuR 4 µM, Ctrl (gray) and PiC KD (light red). *Right*: Quantification of the mitochondrial Ca^{2+} uptake (n = 9/experimental condition).

(B) Representative time course of the mitochondrial matrix Ca^{2+} concentration ($[Ca^{2+}]_m$) upon addition of a 10 µM $CaCl_2$ bolus (10Ca) in suspensions of Ctrl (black) and PiC KD (red) skeletal muscle mitochondria, and in presence of RuR 4 µM, Ctrl (gray) and PiC KD (light red). *Right*: Quantification of the $[Ca^{2+}]_m$ 30 s after the $CaCl_2$ bolus (n = 9/experimental condition).

(C) Representative time course of the mitochondrial clearance, measured as $[Ca^{2+}]_c$, and the $[Ca^{2+}]$m rise upon addition of a 10 µM $CaCl_2$ bolus (10Ca) in suspensions of Ctrl (black), PiC KD (red) mitochondria and PiC KD mitochondria in presence of RuR 5 nM (dark red). *Right*: Quantification of the mitochondrial Ca^{2+} uptake (n = 3/experimental condition).

(D) Representative time course of the mitochondrial matrix Ca^{2+} concentration ($[Ca^{2+}]_m$) upon addition of a 10 µM $CaCl_2$ bolus (10Ca) in suspensions of Ctrl (black), PiC KD (red) mitochondria and PiC KD mitochondria in the presence of RuR 5 nM (dark red). *Right*: Quantification of the $[Ca^{2+}]_m$, 30 s after the $CaCl_2$ bolus (n = 3/experimental condition).

All bar charts: individual data points are shown, and bars represent mean ± s.e.m. Statistical comparison: one-way or two-way ANOVA, **p*<0.05, ***p*<0.01, ****p*<0.001. ‡ = ****p*<0.001 *vs.* condition without RuR. N.S.: not significant.

Figure 3

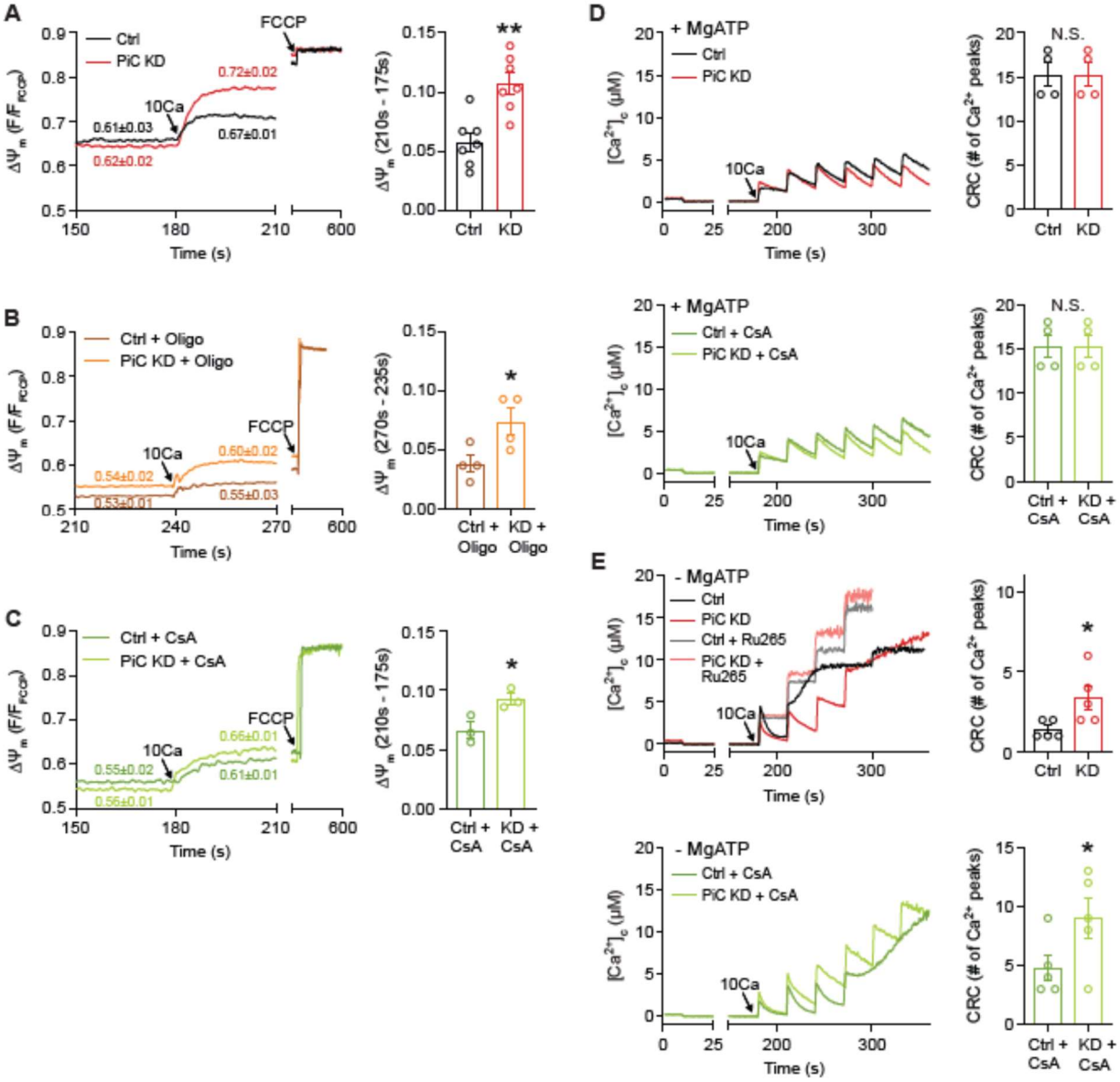
A
Ctrl
PiC KD
FCCP
10Ca
0.72±0.02
0.61±0.03
0.67±0.01
0.62±0.02
Time (s)
**
Ctrl
KD
B
Ctrl + Oligo
PiC KD + Oligo
FCCP
10Ca
0.60±0.02
0.54±0.02
0.55±0.03
0.53±0.01
Time (s)
*
Ctrl + Oligo
KD + Oligo
C
Ctrl + CsA
PiC KD + CsA
FCCP
10Ca
0.66±0.01
0.55±0.02
0.61±0.01
0.56±0.01
Time (s)
*
Ctrl + CsA
KD + CsA
D
+ MgATP
Ctrl
PiC KD
10Ca
Time (s)
N.S.
Ctrl
KD
+ MgATP
Ctrl + CsA
PiC KD + CsA
10Ca
Time (s)
N.S.
Ctrl + CsA
KD + CsA
E
- MgATP
Ctrl
PiC KD
Ctrl + Ru265
PiC KD + Ru265
10Ca
Time (s)
*
Ctrl
KD
- MgATP
Ctrl + CsA
PiC KD + CsA
10Ca
Time (s)
*
Ctrl + CsA
KD + CsA

Figure 3: PiC-depleted mitochondria exhibit increased $\Delta\Psi_m$ depolarization and increased CRC in response to Ca^{2+} uptake.

(A) Mitochondrial membrane potential ($\Delta\Psi_m$) measurements using TMRM, in suspensions of Ctrl (black) and PiC KD (red) mitochondria. TMRM was used in de-quench mode, therefore, the direction of the polarization is downward. FCCP was used to fully dissipate $\Delta\Psi_m$. *Right*: Quantification of $\Delta\Psi_m$ 30 s after the $CaCl_2$ bolus (n = 7/genotype).

(B) $\Delta\Psi_m$ measurements in suspensions of Ctrl (brown) and PiC KD (orange) mitochondria, in presence of oligomycin (Oligo). *Right*: Quantification of $\Delta\Psi_m$ 30 s after the $CaCl_2$ bolus (n = 3/ genotype).

(C) $\Delta\Psi_m$ measurements in suspensions of Ctrl (green) and PiC KD (light green) mitochondria, in presence of cyclosporin A (CsA). *Right*: Quantification of $\Delta\Psi_m$ 30 s after the $CaCl_2$ bolus (n = 3/ genotype).

(D) Evaluation of Ca^{2+} overload-induced mitochondrial PTP opening in suspensions Ctrl (black) and PiC KD (red) mitochondria suspensions in ICM containing Mg-ATP, and in the presence of CsA, Ctrl (green) and PiC KD (light green) *(bottom*). $[Ca^{2+}]_c$ was recorded during repetitive addition (every 30 s) of $CaCl_2$ boluses (10 µM each). *Right*: Quantification of the Ca^{2+} retention capacity (CRC) (n = 5/experimental condition).

(E) Evaluation of Ca^{2+} overload-induced mitochondrial PTP opening in suspensions Ctrl (black) and PiC KD (red) mitochondria suspensions in ICM without Mg^{2+}-ATP, and in the presence of Ru265 (Ctrl, light gray and PiC, light red) and in the presence of CsA, Ctrl (green) and PiC KD (light green) *(bottom*). $[Ca^{2+}]_c$ was recorded during repetitive addition (every 30 s) of $CaCl_2$ boluses (10 µM each). *Right*: Quantification of the Ca^{2+} retention capacity (CRC) (n = 4/experimental condition).

All bar charts: individual data points are shown, and bars represent mean ± s.e.m. Statistical comparison: unpaired t-test, **p*<0.05, ***p*<0.01. N.S.: not significant.

Figure 4

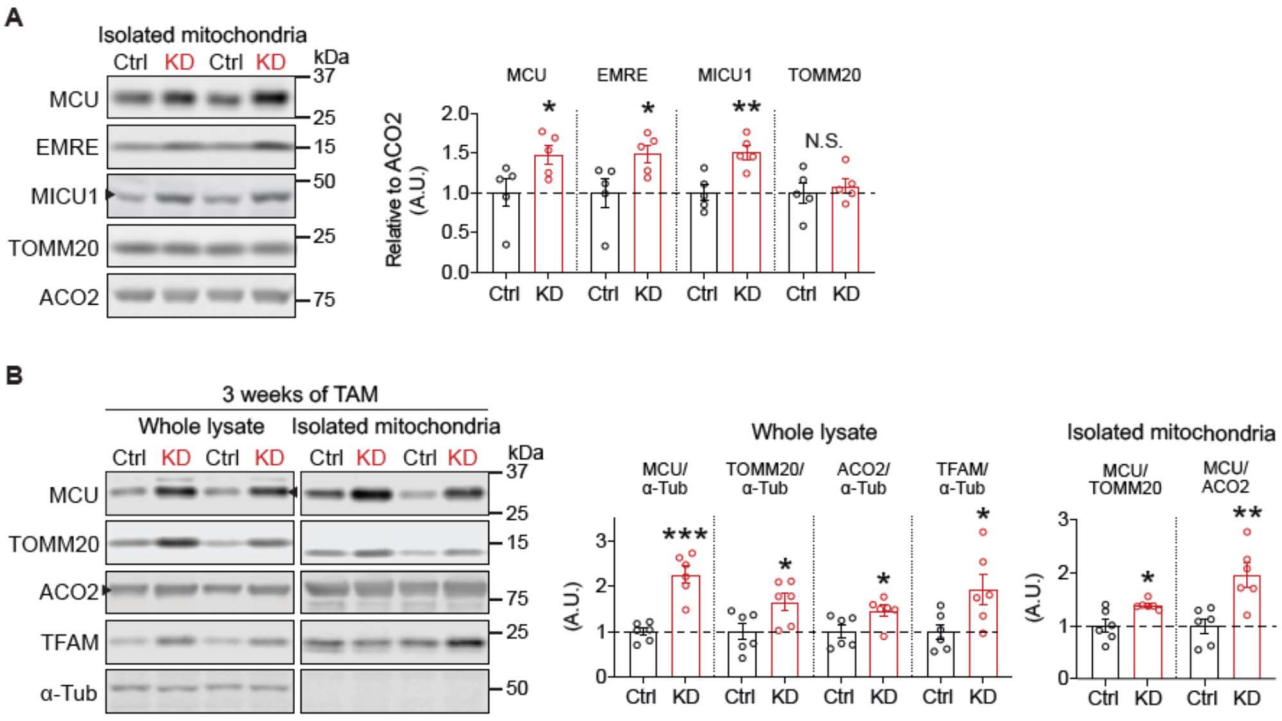

Figure 4: Abundance of mtCU is increased in PiC-depleted muscle

(A) Representative immunoblots of MCU, EMRE, MICU1, TOM20 and ACO2 used as a loading control, in isolated mitochondria from Ctrl and PiC KD muscles. *Right*: Averaged values of MCU, TOM20, ACO2 and TFAM relative to α-Tubulin for whole lysate and MCU/TOM20 and MCU/ACO2 for isolated mitochondria (n = 6/genotype).

(B) Representative immunoblots of MCU, TOM20, ACO2, TFAM and α-Tubulin (loading control) using whole lysates (quadriceps) and isolated mitochondria from Ctrl and PiC KD skeletal muscle. *Right*: Averaged values of MCU, TOM20, ACO2 and TFAM relative to α-Tubulin for whole lysate and MCU/TOM20 and MCU/ACO2 for isolated mitochondria (n = 6/genotype).

All bar charts: individual data points are shown, and bars represent mean ± s.e.m. Statistical comparison: unpaired t-test, **p*<0.05, ***p*<0.01, ****p*<0.001. N.S.: not significant.

Figure 5

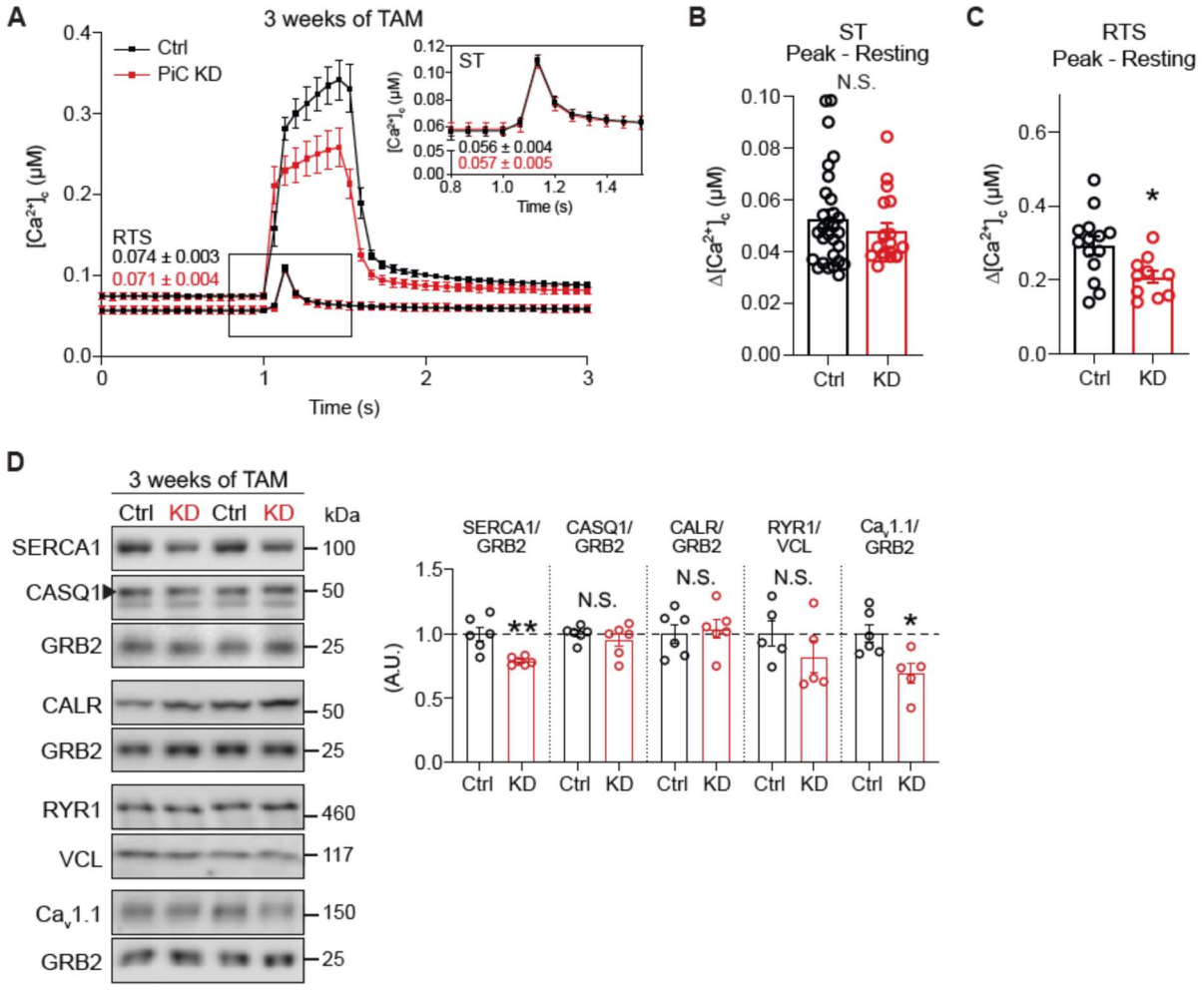

Figure 5: PiC-depleted myofibers have decreased $[Ca^{2+}]_c$ elevation during tetani

A) Averaged traces of $[Ca^{2+}]_c$ levels during single twitch (ST) repetitive tetanic stimulation (RTS), from Ctrl (black) and PiC KD (red). Resting $[Ca^{2+}]_c$ values are shown above the traces. *Inset*: Averaged traces of $[Ca^{2+}]_c$ levels during single twitch (ST), from Ctrl (black) and PiC KD (red). Resting $[Ca^{2+}]_c$ values are shown below the traces.

B) Quantification of $[Ca^{2+}]_c$ peak during ST (n = 29 Ctrl and 19 PiC KD).

C) Quantification of $[Ca^{2+}]_c$ peak during RTS (n = 14 Ctrl and 10 PiC KD).

D) Representative immunoblots of sarcoplasmic reticulum and plasma membrane Ca^{2+} handling proteins (SERCA1, calsequestrin (CASQ1), calreticulin (CALR), RYR1 and Cav1.1). GRB2 and vinculin (VCL): loading controls. *Right*: Averaged values SERCA1, CASQ1, CALR and Cav1.1 relative to α-Tubulin (n = 6 per genotype) and RyR1 relative to VCL (n = 5/genotype).

All bar charts: individual data points are shown, and bars represent mean ± s.e.m. Statistical comparison: unpaired t-test, *p<0.05, **p<0.01. N.S.: not significant.

Figure 6

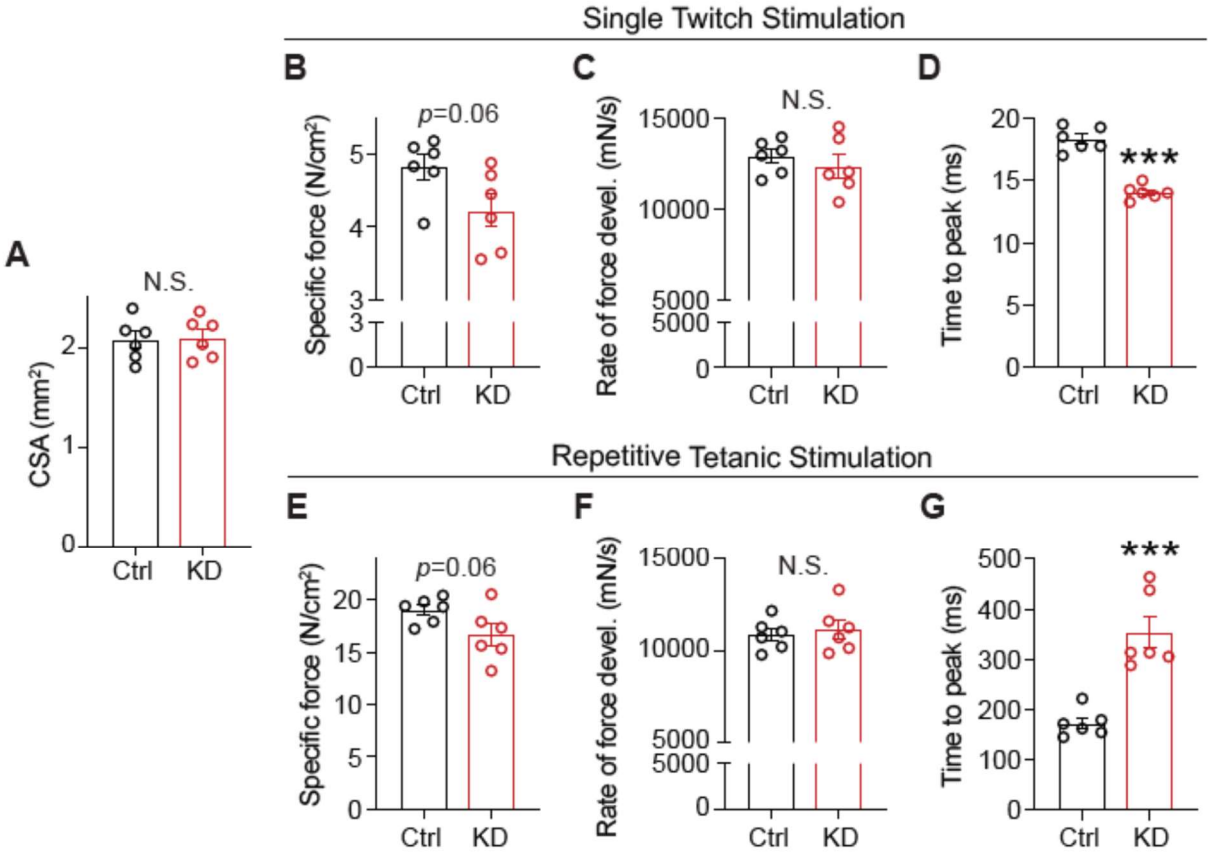
Single Twitch Stimulation
A
N.S.
CSA (mm²)
Ctrl
KD
B
p=0.06
Specific force (N/cm²)
C
N.S.
Rate of force devel. (mN/s)
D
***
Time to peak (ms)
Repetitive Tetanic Stimulation
E
p=0.06
Specific force (N/cm²)
F
N.S.
Rate of force devel. (mN/s)
G
***
Time to peak (ms)

Figure 6: PiC-depleted myofibers exhibit delayed time-to-peak in response to a tetani

(A) Measured cross-sectional area of extensor digitorum longus (EDL) muscle used for ex vivo force measurements in samples from Control (Ctrl) and PiC KD (KD) mice.

(B), (E) Specific force measured during single twitch stimulation, or repetitive tetanic stimulation, respectively, of EDL.

(C), (F) Rate of force development during single twitch stimulation, or repetitive tetanic stimulation, respectively, of EDL.

(D), (G) Time-to-peak in response to single twitch stimulation, or repetitive tetanic stimulation, respectively.

All bar charts: individual data points are shown, and bars represent mean ± s.e.m. Statistical comparison: unpaired t-test, ***p<0.001. N.S.: not significant, n=5/genotype.

Figure 7

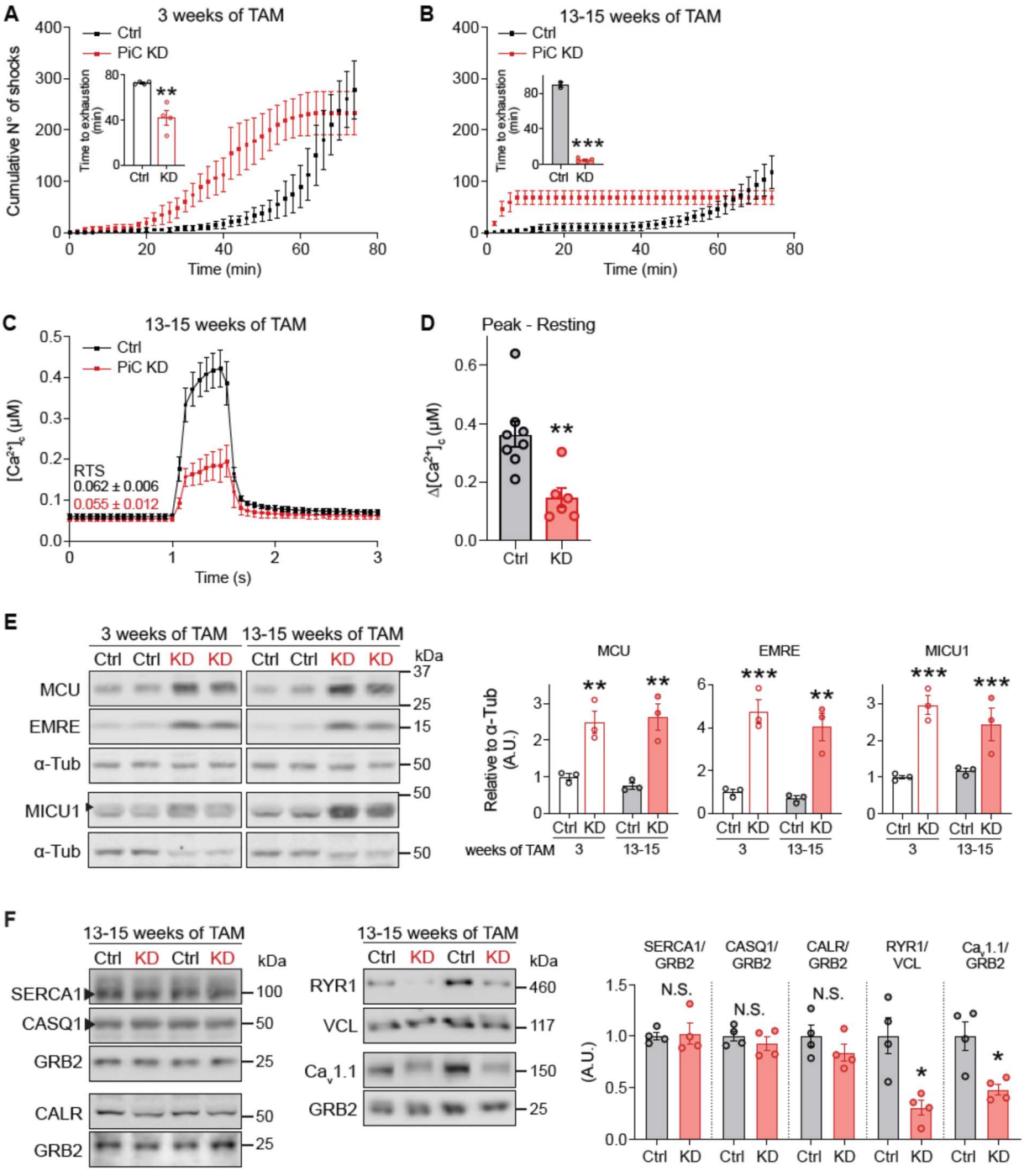
A
3 weeks of TAM
Ctrl
PiC KD
Cumulative N° of shocks
Time to exhaustion (min)
Ctrl KD
**
Time (min)
B
13-15 weeks of TAM
Ctrl
PiC KD
Time to exhaustion (min)
Ctrl KD
***
Time (min)
C
13-15 weeks of TAM
Ctrl
PiC KD
[Ca2+]c (μM)
RTS
0.062 ± 0.006
0.055 ± 0.012
Time (s)
D
Peak - Resting
Δ[Ca2+]c (μM)
**
Ctrl KD
E
3 weeks of TAM
13-15 weeks of TAM
Ctrl Ctrl KD KD Ctrl Ctrl KD KD
kDa
MCU
EMRE
α-Tub
MICU1
α-Tub
37
25
15
50
50
50
MCU
EMRE
MICU1
Relative to α-Tub (A.U.)
Ctrl KD Ctrl KD
weeks of TAM 3 13-15
F
13-15 weeks of TAM
Ctrl KD Ctrl KD kDa
SERCA1
CASQ1
GRB2
CALR
GRB2
100
50
25
50
25
13-15 weeks of TAM
Ctrl KD Ctrl KD kDa
RYR1
VCL
Cav1.1
GRB2
460
117
150
25
SERCA1/ GRB2
CASQ1/ GRB2
CALR/ GRB2
RYR1/ VCL
Cav1.1/ GRB2
N.S.
(A.U.)
Ctrl KD

Figure 7: PiC-depleted myofibers have decreased $[Ca^{2+}]_c$ elevation during tetani

(A), (B) Treadmill running by 13 week-old mice (3 weeks after Tam treatment, n=4), and by 22-24 week-old mice (13-15 weeks after Tam treatment; n=5). Time course shows cumulative number of visits to the shock grid during the run. Plateau indicates that mice no longer ran and were removed from the treadmill. Inset: time to exhaustion.

(C) Averaged traces of $[Ca^{2+}]_c$ levels during repetitive tetanic stimulation from Ctrl (black) and PiC KD (red). Resting $[Ca^{2+}]_c$ values are shown above the traces. N=8/genotype.

(D) Quantification of $[Ca^{2+}]_c$ peak during RTS (n = 8/genotype).

(E) Representative immunoblots of MCU, EMRE and MICU1, and α-Tubulin (loading control) in whole muscle (quadriceps) lysates. *Right*: Quantification (n = 3/genotype).

(F) Expression of sarcoplasmic reticulum and plasma membrane Ca^{2+} handling proteins (SERCA1, calsequestrin (CASQ1), calreticulin (CALR), RYR1 and Cav1.1). GRB2 and vinculin (VCL): loading controls. *Right*: Quantification, n = 4/genotype.

All bar charts: individual data points are shown, and bars represent mean ± s.e.m. Statistical comparison: unpaired t-test, **p*<0.05, ***p*<0.01, ****p*<0001. N.S.: not significant.

Suppl. Figure 1

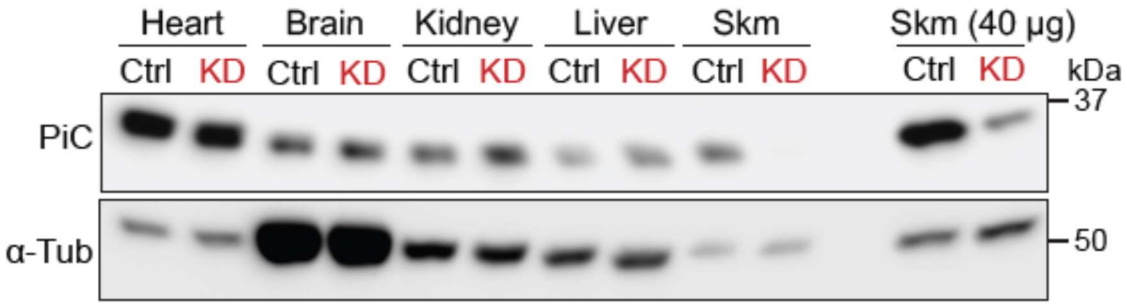

Suppl. Fig. 1: Immunoblot detection of PiC protein in lysates from several tissues, in $PiC^{fl/fl}$ control (Ctrl) mice and in mice with skeletal muscle-specific PiC depletion (KD).

Suppl. Figure 2

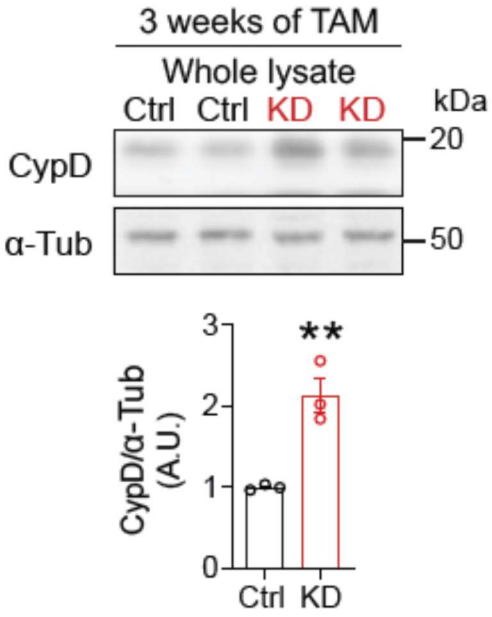

Suppl. Fig. 2: Elevated CypD expression in quadriceps lysates from skeletal PiC KD mice. Values are mean±sem (n=3). Unpaired t-test, $^{**}p < 0.01$.

Suppl. Figure 3

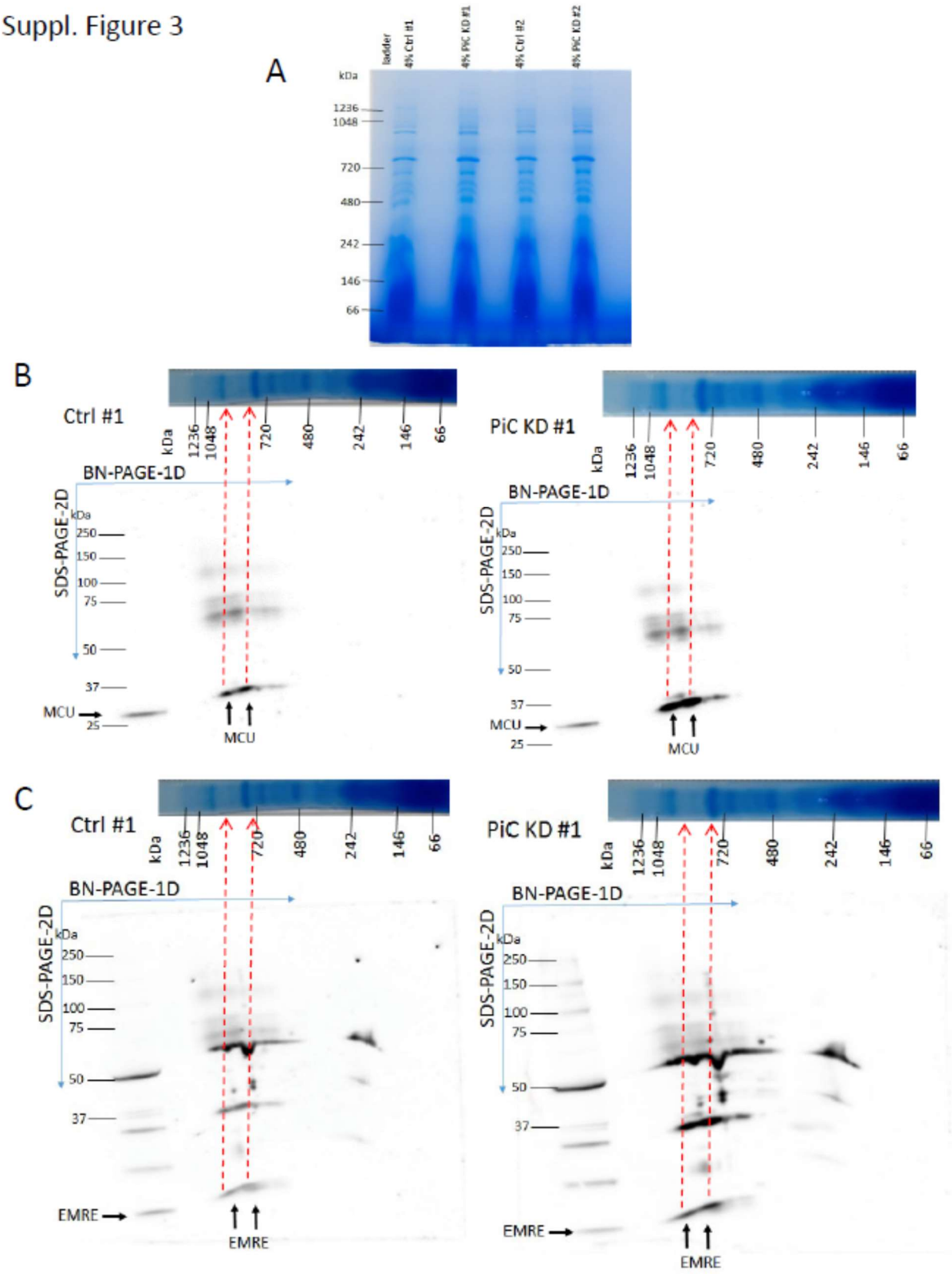

Suppl. Fig. 3

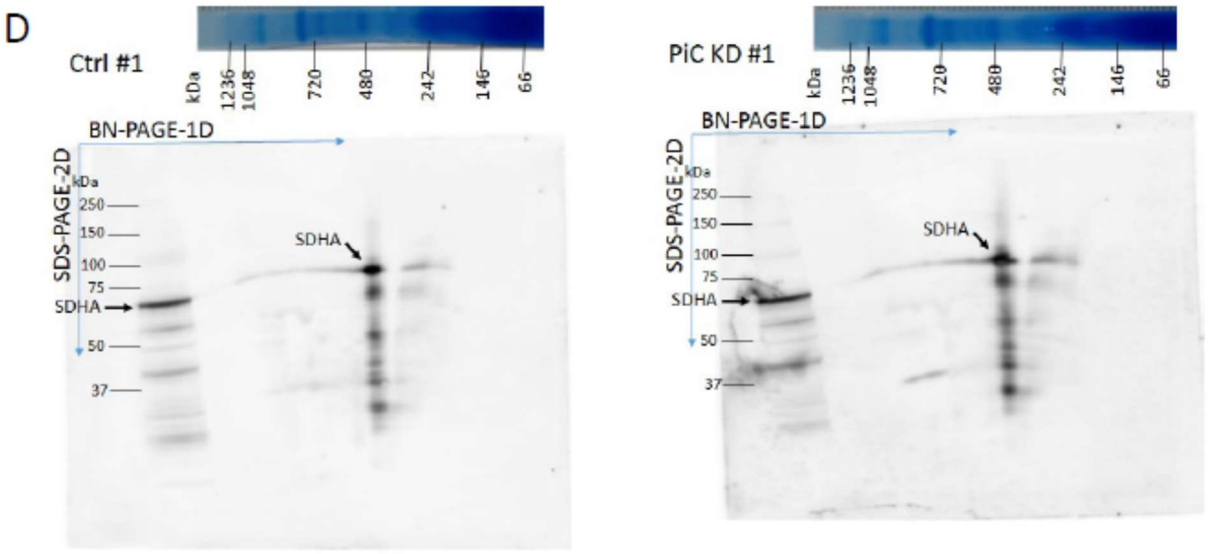
D
Ctrl #1
kDa
1236
1048
720
480
242
146
66
BN-PAGE-1D
SDS-PAGE-2D
kDa
250
150
100
75
SDHA
50
37
SDHA
PiC KD #1
kDa
1236
1048
720
480
242
146
66
BN-PAGE-1D
SDS-PAGE-2D
kDa
250
150
100
75
SDHA
50
37
SDHA

Suppl. Fig. 3

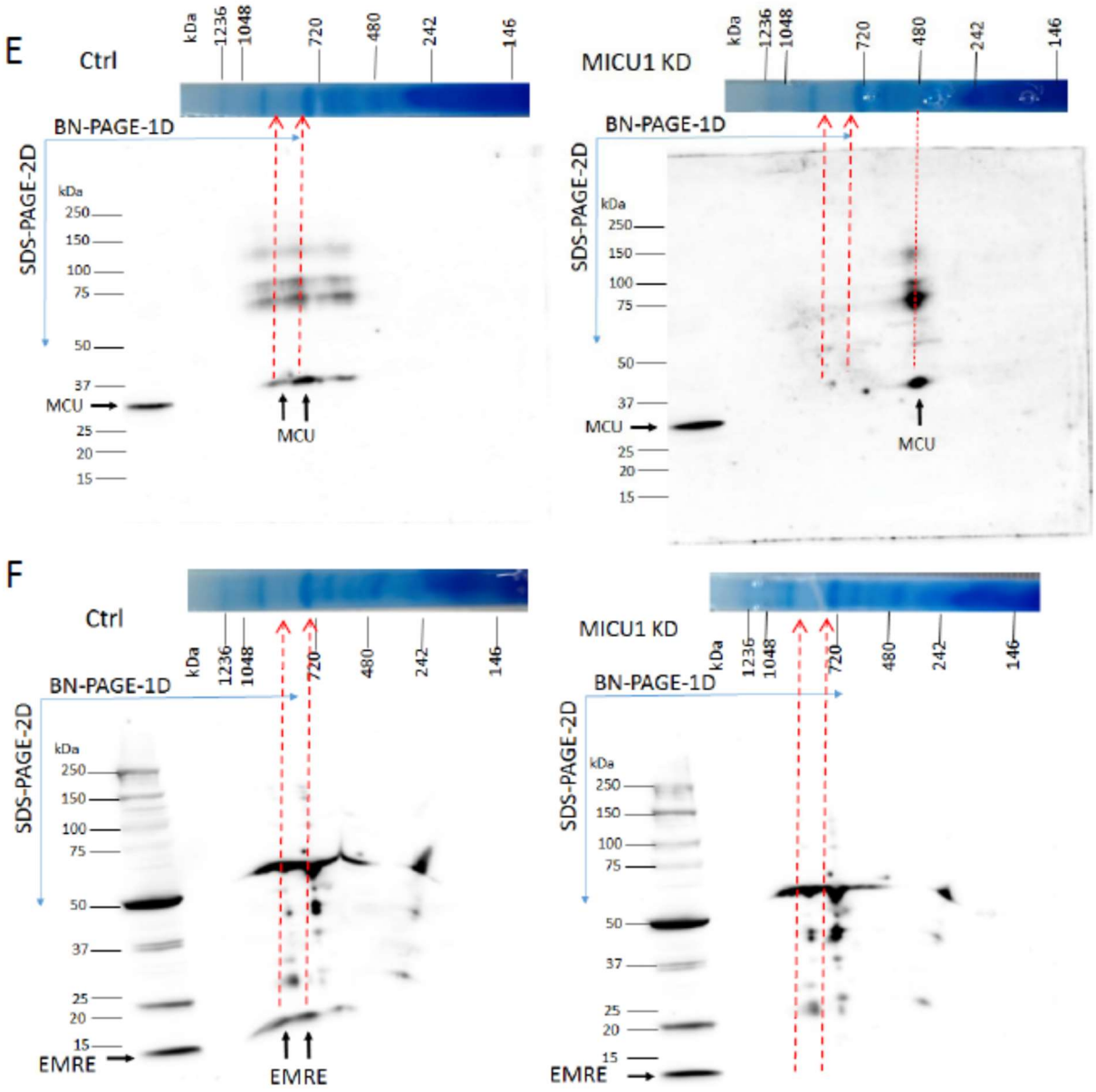
E
Ctrl
MICU1 KD
kDa
1236
1048
720
480
242
146
BN-PAGE-1D
SDS-PAGE-2D
250
150
100
75
50
37
25
20
15
MCU
F
Ctrl
MICU1 KD
EMRE

Suppl. Fig. 3: Evaluation of MCU and EMRE using non-denaturing followed by 2nd dimension denaturing electrophoresis.

(A) Coomassie-stained non-denaturing gel showing electroporesed skeletal muscle mitochondria from control (Ctrl) and PiC KD (KD) mice.

(B) (C) (D) Separate lanes containing Ctrl and KD skeletal muscle mitochondria samples were excised, rotated 90° (i.e., the gel pictured at the top of each membrane) then electrophoresed through a denaturing gel. Shown are representative runs for a Ctrl and a KD sample. Membranes were probed with antibodies against MCU **(B)**, EMRE **(C)** and SDHA (D). SDHA serves as a loading control, as does the Coomassie-stained gel shown in **(A)**. On each membrane, the left-most lane contains a molecular weight marker as well as a sample of isolated mitochondria from a control mouse that was immediately prepared in denaturing sample buffer. In **(B)** and **(C)**: vertical red line points to the approximate molecular weight of the protein complex from which the band on the denaturing gel was obtained.

(E) (F) The same experiment as shown in **(B)** and **(C)** was conducted using skeletal muscle mitochondria isolated from Ctrl and mice with striated muscle-specific depletion of the mtCU regulator, MICU1, which also shows substantial depletion of EMRE and to a lesser extent MCU. Note the absence in the MICU1-depleted sample of MCU-immunoreactive bands corresponding to the two higher molecular weight areas of the non-denaturing gel **(E)**. Note, too, the absence of detectable EMRE **(F)**.

Suppl. Figure 4

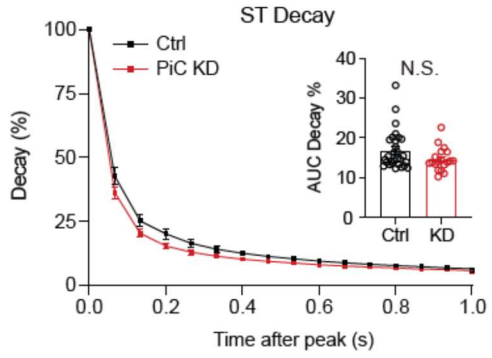

Suppl. Fig 4: Decay kinetic of [Ca^{2+}] in FDB muscle fibers from control (Ctrl) and PiC KD mice. Values are mean±sem (n = 29 Ctrl and 19 PiC KD). No difference between the genotypes.

<u>PART 2</u> Aim 3: Generation of a TAT fusion protein to deliver PiC: correct compartmentalization to the inner mitochondrial membrane and ability to rescue PiC deficiency phenotypes

Introduction

Modern medicine offers no cure for genetic mitochondrial disorders and the usual treatment is only palliative. We proposed in this research the concept for the treatment of mitochondrial disorders using Protein Replacement Therapy, by the delivery of a wild type mitochondrial protein directly to its sub-cellular location, in the form of a fusion protein. Our approach is to fuse the normal protein, mutated in a known mitochondrial disease, with the delivery peptide TAT, which will lead the protein into the cells and their mitochondria where it will substitute for the mutated endogenous protein or allow the expression of a protein that cannot be expressed because of a mutation. The most well-known, investigated and tested delivery peptide is the HIV-transactivator of transcription (TAT) peptide. TAT-fusion proteins are rapidly and efficiently introduced into cultured cells, intact tissue, live tissues and traverse also the mitochondrial membranes. This approach was tested by us before and proven to work, for mitochondrial matrix soluble proteins.

The approach of protein replacement was as yet not tested for mitochondrial-membrane proteins. In this research we focused on the PiC, localized to the IMM. Humans have a documented alternatively spliced exon 3A and 3B, generating two PiC isoforms, A and B. Thus, we designed and construct both TAT-MTS-PiC-A and TAT-MTS-PiC-B *human* isoforms (TAT-PiCA was described last year and is further discussed here; generation of TAT-PiC-B is underway, and not discussed here). The natural mitochondrial targeting sequence (MTS) of PiC (49 aa) was used.

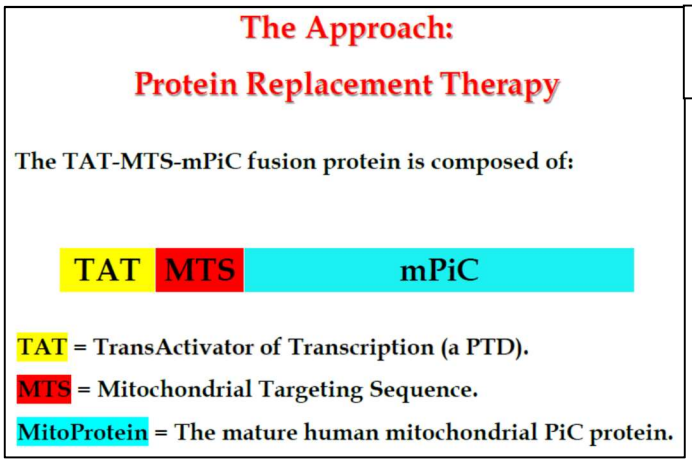

Figure 1: Schematic presentation of TAT-MTS-mPiCA fusion protein.

Here our goal was to construct and test TAT-MTS-PiC fusion proteins as a means of rescuing deleterious phenotypes caused by mPiC loss. A schematic presentation of the fusion protein is demonstrated in **Figure 1**.

Approach and Results

A. Selection of bacterial systems and generation of TAT-MTS-PIC in inclusion bodies

The first goal was to construct and test TAT-PiC as a means of rescuing deleterious phenotypes caused by PiC loss. Humans (and mice) have a documented alternatively spliced exon 3A and 3B, generating two PiC isoforms, A and B. Thus, we designed and constructed both TAT-PiC-A and TAT-PiC-B *human* isoforms. The natural mitochondrial targeting sequence (MTS) of PiC (49 aa) was used.

The sequence encoding the chimeric protein was inserted into a pet28 expression vector under the control of the T7 promoter. **Figure 2A** demonstrates the schematic structure of the final chimeric proteins: TAT-MTS-PiC-A and TAT-MTS-PiC-B. The coding sequence of both chimeric proteins was confirmed by sequencing analysis. Full amino acid sequences of TAT-MTS-PiC-A and TAT-MTS-PiC-B fusion protein are shown in **Figure 2B**.

A **TAT-MTS-Mito Protein Fusion Proteins: construct design**

B **Mitochondrial PiC isoforms A & B:**

	TAT-MTS-PiCA	TAT-MTS-PiCB
DNA seq. Length	1188	1185
Amino acids	MGSSHHHHHHSSGLVPRGSHMRKKRRQRRRGSGSFSSVAHLARANPFNTPHL QLVHDGLGDLRSSSPGPTGQPRRPRNLAAAAVEEQYSCDYGSGRFFILCGLGG IISCGTTHTALVPLDLVKCRMQVDPQKYKGIFNGFSVTLKEDGVRGLAKGWA PTFLGYSMQGLCKFGFYEVFKVLYSNMLGEENTYLWRTSLYLAASASAEFFA DIALAPMEAAKVRIQTQPGYANTLRDAAPKMYKEEGLKAFYKGVAPLWMRQ IPYTMMKFACFERTVEALYKFVVPKPRSECSKPEQLVVTFVAGYIAGVFCAIV SHPADSVVSVLNKEKGSSASLVLKRLGFKGVWKGLFARIIMIGTLTALQWFIY DSVKVYFRLPRPPPPEMPESLKKKLGLTQ first methionine His tag TAT mts PiCVar1	MGSSHHHHHHSSGLVPRGSHMRKKRRQRRRGSGSFSSVAHLARANPFNTPHL QLVHDGLGDLRSSSPGPTGQPRRPRNLAAAAVEEYSCEFGSAKYYALCGFGG VLSCGLTHTAVVPLDLVKCRMQVDPQKYKGIFNGFSVTLKEDGVRGLAKGW APTFLGYSMQGLCKFGFYEVFKVLYSNMLGEENTYLWRTSLYLAASASAEFF ADIALAPMEAAKVRIQTQPGYANTLRDAAPKMYKEEGLKAFYKGVAPLWMR QIPYTMMKFACFERTVEALYKFVVPKPRSECSKPEQLVVTFVAGYIAGVFCAI VSHPADSVVSVLNKEKGSSASLVLKRLGFKGVWKGLFARIIMIGTLTALQWFI YDSVKVYFRLPRPPPPEMPESLKKKLGLTQ first methionine His tag TAT mts PiCVar2
Length aa	395	394
MW	43868.05	43731.90

Figure 2. **TAT-PiC fusion protein design for isoforms A and B of PiC**. Panel A presents a schematic of the construct design that includes a mitochondrial targeting sequence (MTS). Panel B shows the actual sequences for both constructs.

At first, we performed experiments with the TAT-MTS-PiCA fusion protein. The TAT-MTS-PiC-A chimeric protein was expressed in various bacterial expression systems and under different conditions (not shown). The most successful expression system proved to be expression in the HMS

bacterial strain, growth at 37ºC following induction with 1mM IPTG for 2-3 hrs at 37ºC.

Following expression, various subcellular fractions were prepared: whole cell extract (WCE), soluble fraction (Sol) and inclusion bodies (IB), separated on SDS-PAGE, and characterized both by Coomassie blue staining and by immunoblot analyses, using anti-His and human anti-PiC antibodies (Sigma). Coomassie blue staining revealed bands with estimated masses corresponding to those of the over-expressed protein: ~43kDa. Western blot performed with antibodies specific to His (**Figure 3**) and human PiC (not shown) confirmed the identity of the fusion protein. As expected, being an inner membrane mitochondrial protein, when analyzed by immunoblot, the subcellular fraction that held a larger portion of the TAT-MTS-PiC-A fusion protein was the IB in the bacteria (not shown). These analyses confirm the successful expression of the in-frame, full-length fusion protein.

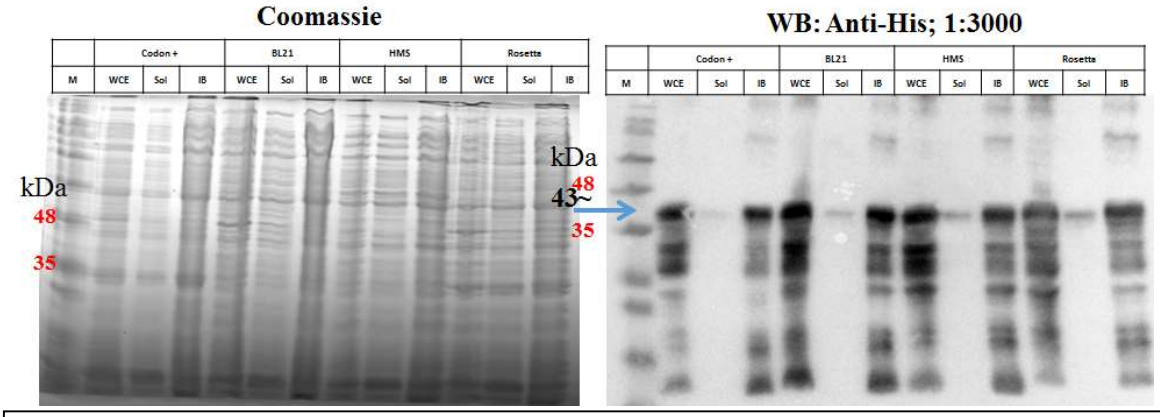

Figure 3. **TAT-PiCA is found in inclusion bodies**. Subcellular fractions (WCE: whole cell extract; Sol: soluble fraction; IB: inclusion bodies) were electrophoresed and probed with Anti-His antibodies (right panel). The major band was found at ~43 kDa which is the calculated molecular weight for the His-tagged TAT-PiCA protein. Coomassie blue-stained gel (left panel) shows electrophoresed protein in all fractions.

A frozen pate of the bacteria were thawed and suspended in lysis buffer (20 mM Tris-HCl, pH 8.0; 0.05 M NaCl; 0.2 mg/ml lysozyme; 1 mM phenylsullfonyl fluoride (PMSF)) for 30 minutes at room temperature, followed by sonication (the last calibration is using a microfluidezer to disrupt the bacterial cells instead of using a sonicator). A sample was taken from the lysed cells and marked as whole cell extract (WCE). The rest of the cells were then centrifuged at 17,500 g for 30 min. The supernatant (marked as soluble fraction; sol) was removed and the pellet (containing inclusion bodies) was suspended in denaturation buffer (6 M urea; 20 mM Tris-HCl, pH 8.8; 0.05 M NaCl; 5mM β-mercaptoethanol) and continuously stirred for 90 minutes. The solution was cleared by

centrifugation at 17,500 g for 30 min. The supernatant, containing denatured proteins, was collected and marked as inclusion bodies (IB).

The denatured chimeric proteins in 6M urea were filtrated and a final concentration of 10 mM imidazole was added. The protein was subjected to immobilized metal affinity chromatography using 5 ml His-Trap columns, and was eluted with a linear imidazole gradient of 10–500 mm (**Figure 4**, rightmost panel). Again, being a membrane protein, calibration experiments were performed to allow binding of the fusion protein to the affinity column (results not shown). **Figure 4** shows the affinity purification of the TAT-MTS-PiC-A fusion protein.

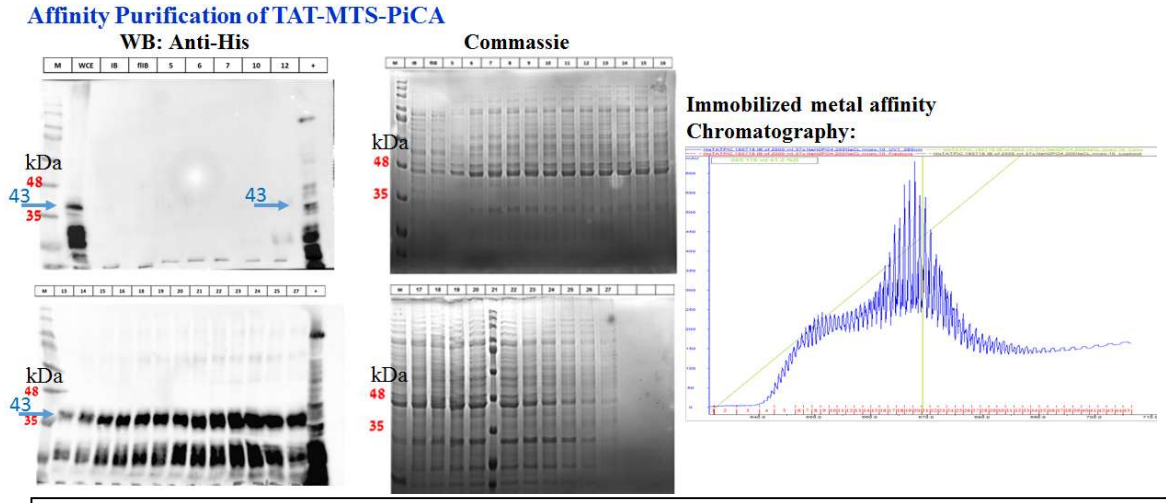

Figure 4. **Affinity chromatography to TAT-PiC-A.** Left upper and lower panels show immunoblot of elution fractions, probed with an anti-His antibody. Labels along the top indicate whole cell lysate (WCE) followed by the numbers of the collected fractions. TAT-PiCA runs at ~43 kDa and appeared most abundantly in fractions 16 through 27. Gels on the right show correctly electrophoresed protein in all fraction, demonstrated using Coomassie blue staining. The rightmost panel displays the chromatogram readout.

B. Purification of TAT-MTS-PiC (A&B) from inclusion bodies

Following expression, as expected, being an inner membrane mitochondrial protein, TAT-MTS-PiC fusion protein was mainly found in inclusion bodies (IB) of the bacterial expressing cells. Therefore, following expression, IB were separated and denatured in 6M urea. The denatured TAT-MTS-PiC fusion proteins in 6 M Urea, were added with 10 mM imidazole. The protein was subjected to immobilized metal affinity chromatography using 5 ml His-Trap columns, and was eluted with a linear imidazole gradient of 10–500 mM. Again, being a membrane protein, calibration experiments were performed to allow binding of the fusion protein to the affinity column (not shown). A key

element for the binding to the affinity column was using NaH_2PO4 in the binding buffer. **Figures 5** demonstrates a typical affinity purification of the TAT-MTS-PiC-A fusion protein.

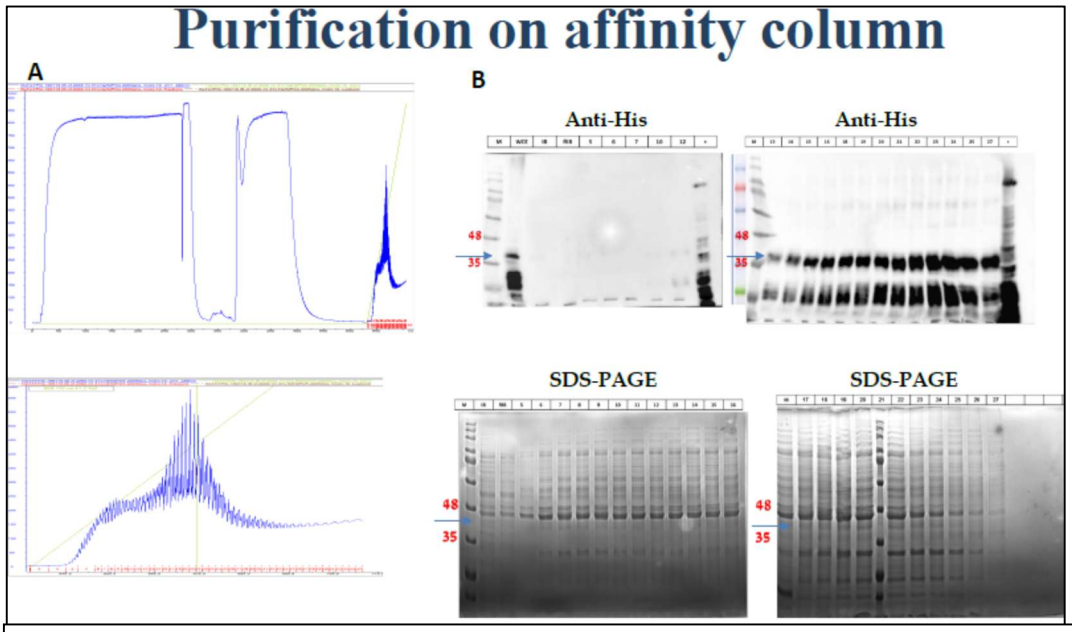

Figure 5: Typical affinity purification of TAT-MTS-mPiCA under denatured conditions (6M Urea). **A**: Column profile; **B**: Lower panel: SDS-PAGE analysis of the affinity column fractions. Upper panel: western blot of affinity column fractions using anti-His antibodies.

The next crucial step was to exchange the buffer to a physiological one, allowing future biological testing of the fusion protein. Calibration experiments helped to define the dialysis buffer for the partial purified protein. We found that this buffer should contain 200 mM L-Arginine (**Fig. 6**). **Fig. 7** summarizes all calibration experiments for purification of the TAT-MTS-mPiCA fusion protein.

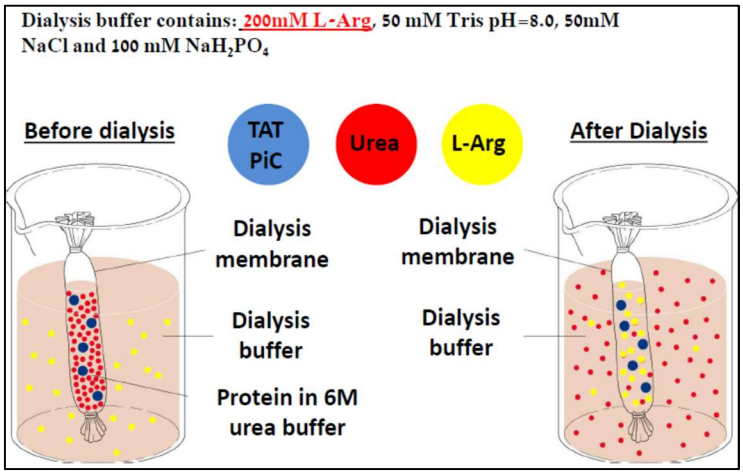

Figure 6: Schematic presentation of the dialysis step in the preparation of TAT-MTS-mPiCA fusion protein, indicating the importance of adding 200mM L-arginine to the protein preparation.

From DNA to protein

Cloning, Expression and partial Purification

Cloning

pET 28 vector

Bacterial expression system, temperature, IPTG concentration

HMS 37°c 1 mM

Lysis buffer

10mM Tris pH=8.0, 100mM NaCl, 100mM NaH_2PO_4, 10% glycerol, 2mM βME

Lysis with-

Microfluidizer

Denaturation buffer

6M Urea, 10mM Tris pH=8.0, 100mM NaCl, 100mM NaH_2PO_4, 2 mM βME

Ni Column binding buffer

"Denaturation buffer" + 5mM imidazole

Ni Column elution buffer

"Denaturation buffer" + 500mM imidazole

Dialysis

200mM L-Arg, 50 mM Tris pH=8.0, 50mM NaCl and 100 mM NaH_2PO_4

Figure 7: Summarizing conditions for purification of the TAT-MTS-mPiCA fusion protein.

Using a similar strategy as that used to generate TAT-MTS-PiC-A, we produced a construct for the B isoform of the PiC fused to TAT, then purified TAT-PiC-B. This was successfully accomplished (**Figure 8**).

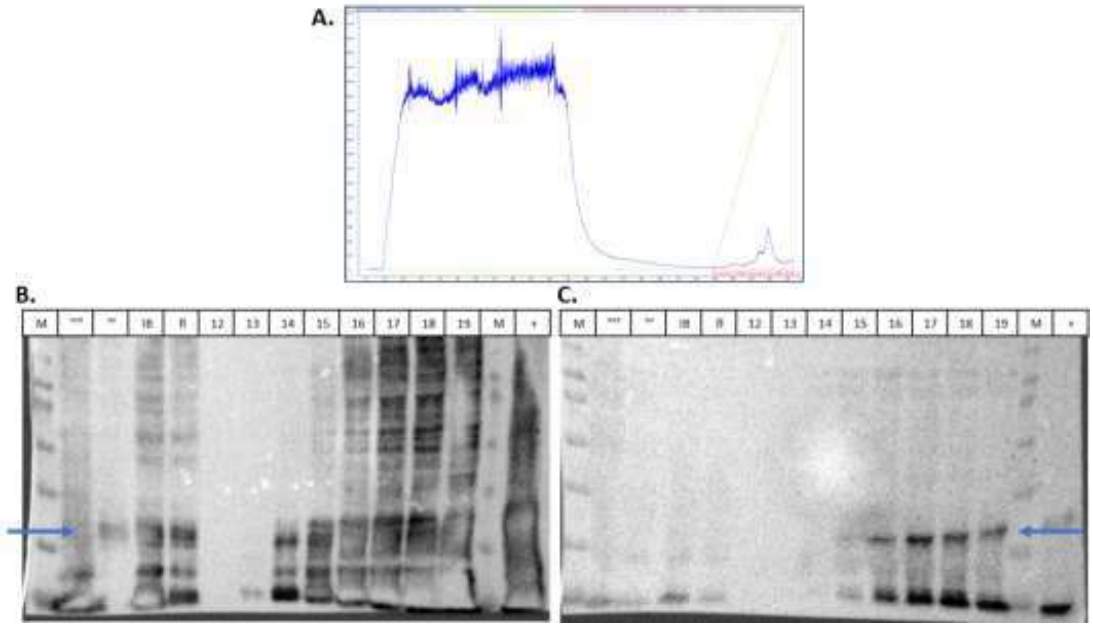

Figure 8: Purification of TAT-MTS-PiCB isoform The TAT-MTS-PiCB isoform of the chimeric protein was constructed, expressed and partially purified.

A. Purification of TAT-PiCB on a His-Trap. column under denatured condition.

B. SDS –gel of the purification on the His-Trap column.

C. Western blot analysis of the purification steps using anti-His antibodies.

C. Partial Purified TAT-MTS-PiC-A fusion protein is not cytotoxic to cultured cells

To ensure that the TAT-MTS-PiC-A fusion protein preparation is safe to be used for further testing, we examined its effect of the viability of cultured cells, as compared to control cells exposed only to the buffer of the fusion protein. As shown in **Figure 9**, TAT-MTS-PiC-A had no cytotoxic effect on the viability of HeLa cells (human cells) at various concentrations of the fusion protein.

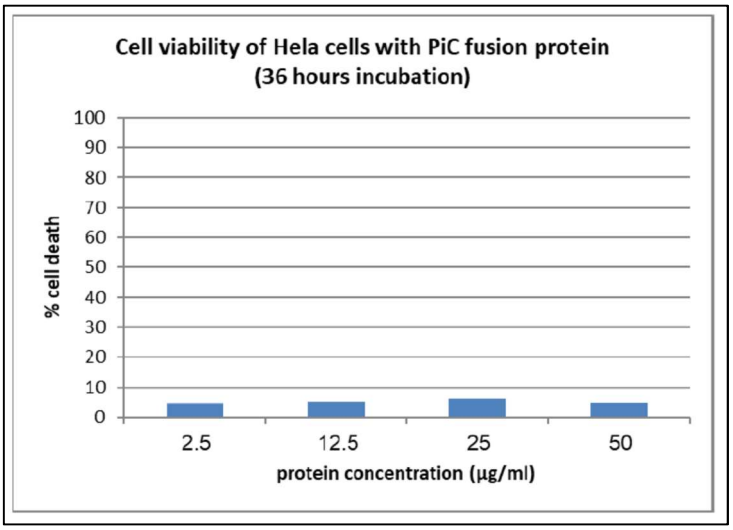

Figure 9: TAT-MTS-mPiCA fusion protein has no cytotoxic effect on the viability of human HeLa cells at various concentrations of the fusion protein.

D. TAT-MTS-PiC-A fusion protein is internalized into cells

We followed the internalization of the TAT-MTS-PiC-A fusion protein into HeLa cells. HeLa cells were incubated with TAT-MTS-PiC-A for 3 hr. We prepared then lysates from control (untreated cells) or treated cells, and followed the existence of the fusion protein using anti-PiC antibodies. As seen in **Figure 10**, the fusion protein was found in the cell lysates, and in larger amounts when added at higher concentrations (dose response). Thus, TAT-MTS-PiC-A is internalized into the cells, following its incubation with cells.

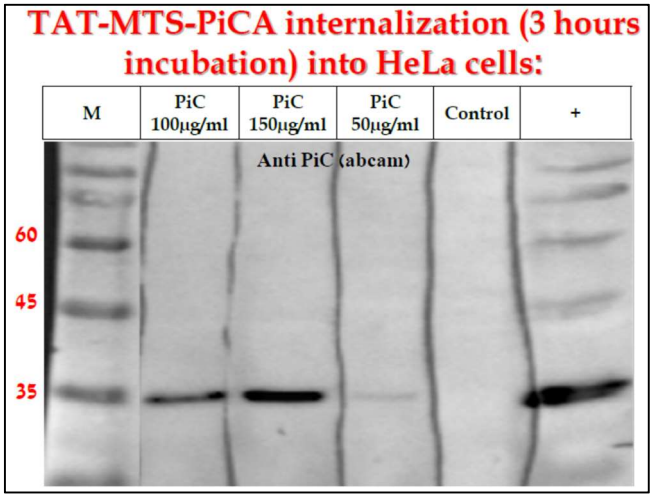

Figure 10: TAT-MTS-PiC-A fusion protein is internalized into cells. HeLa cells were incubated with various concentration of TAT-MTS-mPiCA for 3 hr. We prepared then lysates from control (untreated cells) or treated cells, and followed the existence of the fusion protein using anti-PiC antibodies. It should be pointed out that we used antibodies from Abcam showing the fusion protein at MW of ~35kD. Using another commercial anti-PiC (Protein Tech) the fusion protein was identified at its correct ~43kD (not shown).

E. TAT-MTS-PiC-A added to cells reaches its endogenous location, the IMM

The major question we had to address following TAT-MTS-PiC-A internalization into cells is, will it reach its final cellular destination, the IMM? To address this question, HeLa cells were incubated with TAT-MTS-PiC-A for 3 hr and sub-fractionation was performed (see scheme for sub-fractionation in **Figure 11**).

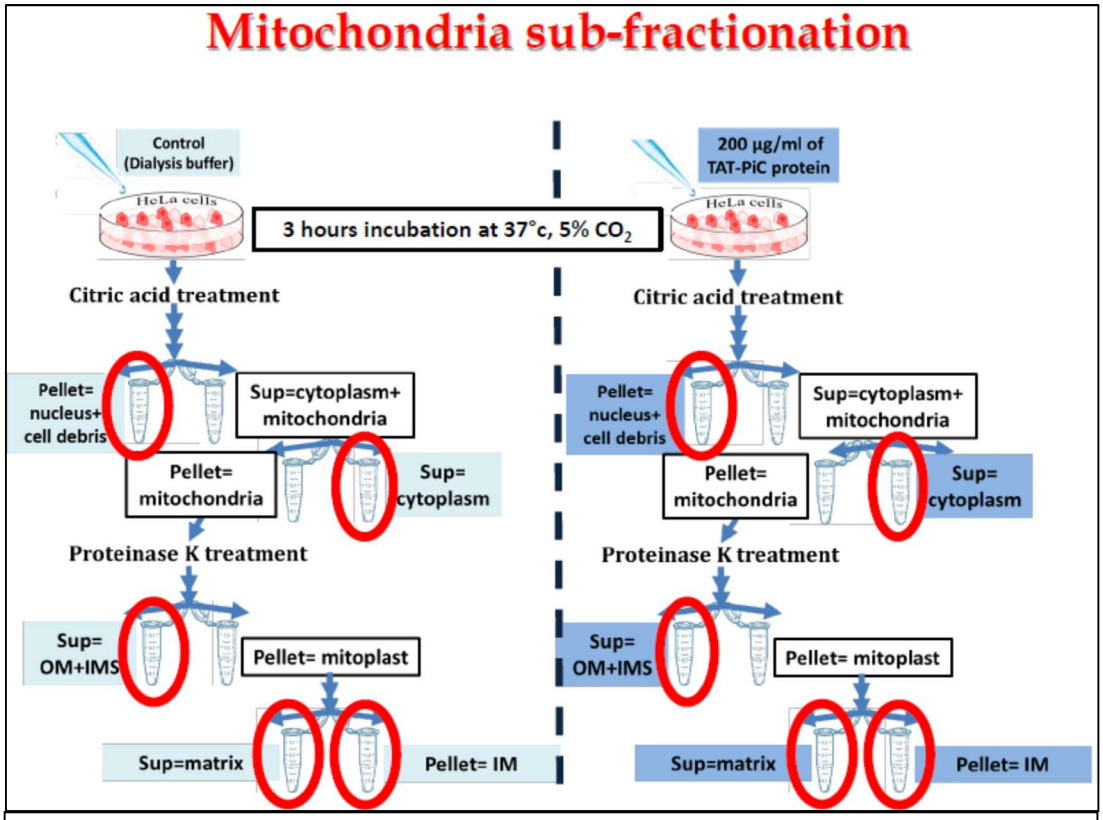

Figure 11: Schematic presentation of mitochondrial sub-fractionation.

The existence of the fusion protein was tested by western blot analysis using anti-PiC antibodies. Purity of the sub-fractions was confirmed by using anti-Tubulin antibodies for the cytosolic sub-fraction, anti-Lamin B antibodies for the nucleus and anti-CoIV for the inner mitochondrial membrane (IMM) sub-fraction. As seen in **Figure 12 (next page)**, TAT-MTS-PiC-A localized to the IMM, with no evidence for its existence in the mitochondrial matrix or mitochondrial outer membranes or intermembrane space. We repeated the these experiments using 3 different cell cultures and as seen in **Figure 13**, in Hela cells, HEK293 cells and HePG2 cells incubated with the fusion protein. In all cell types, the fusion protein entered the cells and reached the IMM.

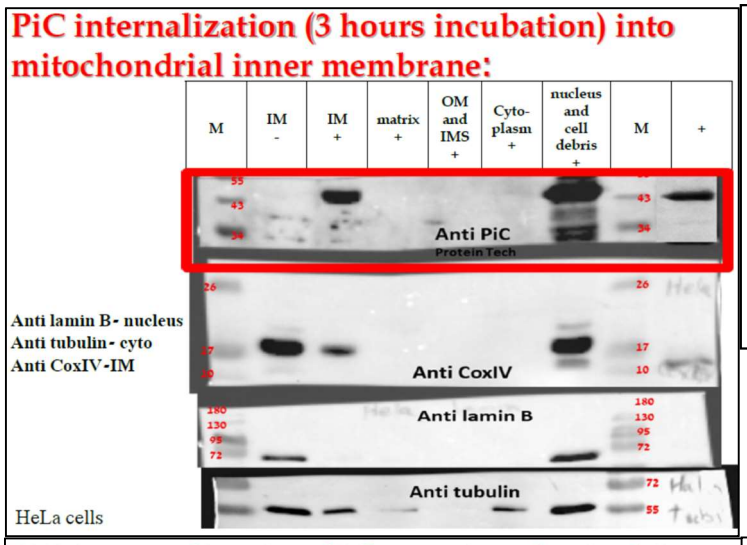

Figure 12: Localization of TAT-MTS-PiC fusion protein within HeLa cells.
TAT-MTS-PiC-A is found in the mitochondrial inner membrane with no evidence for its existence in the mitochondrial matrix or mitochondrial outer membranes + inner membrane space.

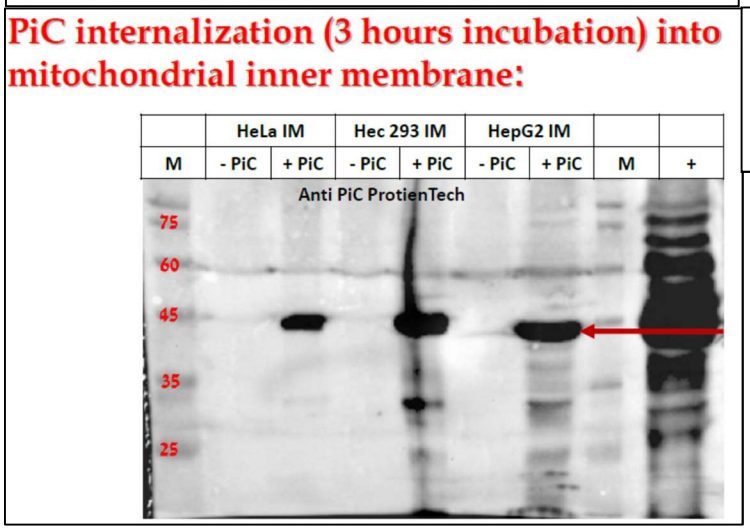

Figure 13: Localization of TAT-MTS-mPiC fusion protein within HEK293, HepG2 and HeLa cells (arrow).

F. Efficacy of TAT-MTS-PiC-A to rescue mitochondria function in cells depleted of PiC

We next tested the ability of TAT-MTS-PiC-A to improve mitochondrial functionality of cells with decreased expression of PiC. As PiC is an essential protein for cells, we could not generate a knock out cell line by the CRISP/Cas9 technology; thus, we used specific si-PiC for transiently lowing the expression of PiC.

Transient transfection with esi-PiC of Hela cells lowered PiC-mRNA levels by more than 85%, as determined by qPCR (**Figure 14: next page**). Transfected cells, at 48hr post transfection, grew slower; showing a 43% reduction in cell number (**Figure 15A, B: next page**). Treatment with TAT-MTS-PiC-A fusion protein for 24hr increased cell growth, resulting in ~15% higher cell numbers at the end of the incubation period (**Figure 15A, B**).

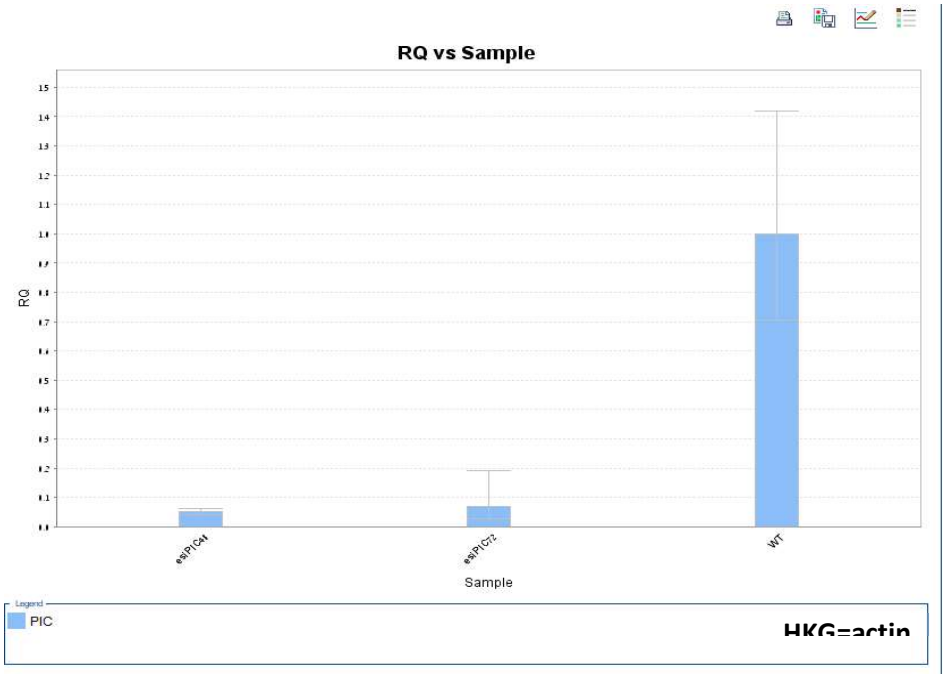

Figure 14. **Transient PiC knockdown (esi-mPiC) lowers mPiC mRNA levels in Hela cells.** Cells were transfected with esi-mPiC (20 nM final concentration per well). After 24 hrs incubation, the media (rich media) was replaced and cell were incubated for an additional 24 or 48 hrs. RNA was isolated at 48 hrs or 72 hrs post infection and qPCR was performed using specific primers for mPiCA.

Figure 15. esi-mPiCA slows proliferation rate of Hela cells. Hela cells were transfected with esi-

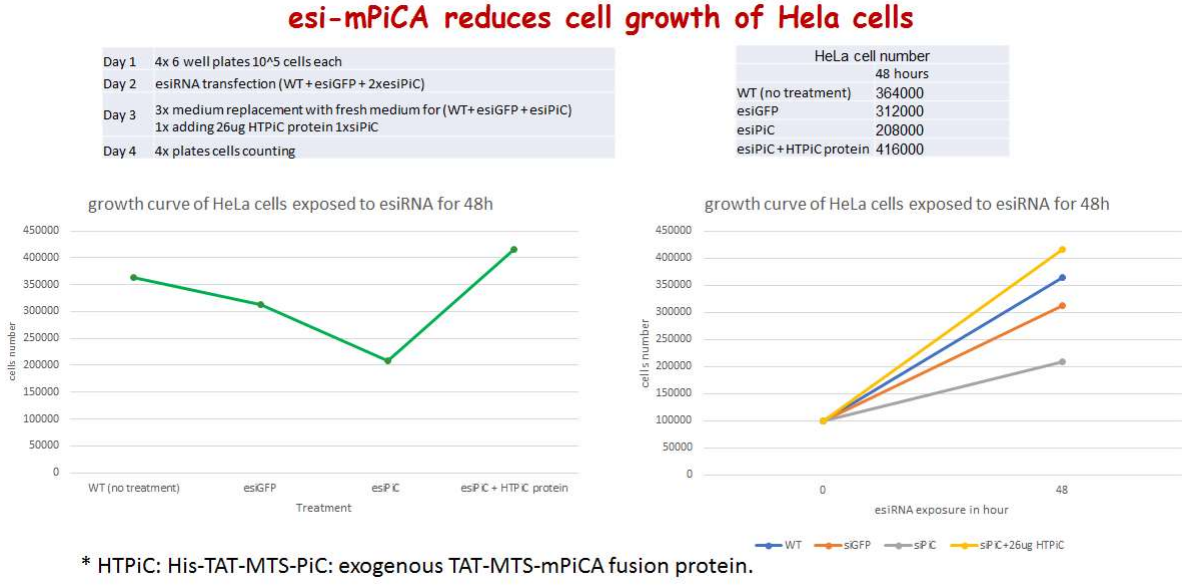

* HTPiC: His-TAT-MTS-PiC: exogenous TAT-MTS-mPiCA fusion protein.

PiCA for 24 hrs. Then, incubation media was changed to rich media and TAT-MTS-mPiC fusion protein was added for an additional 24 hrs, at two concentrations and cell number was determined using trypan blue staining.

We next tested the effect of TAT-MTS-PiC-A fusion protein on mitochondrial activity in Hela cells with lowered expression of PiC (treated with si-PiC) using bioenergetics analyses (**Figure 16**: using Seahorse technology). Treatment with TAT-MTS-PiC-A fusion protein significantly improved mitochondrial bioenergetics as measured by increased O_2 consumption rate (OCR), showing a 3Xfold increase with 10 µg of fusion protein and 9.3Xfold increase following treatment with 20 µg of the fusion protein. Treatment with the fusion protein also increased ATP production; 1.8x and 3.3xfold with 10 µg and 20 µg of the fusion protein respectively (**Figure 16**). These results also demonstrate that improvement of mitochondrial bioenergetics is dose dependent (**Figure 16**). These analyses were repeated 4 time, with similar results.

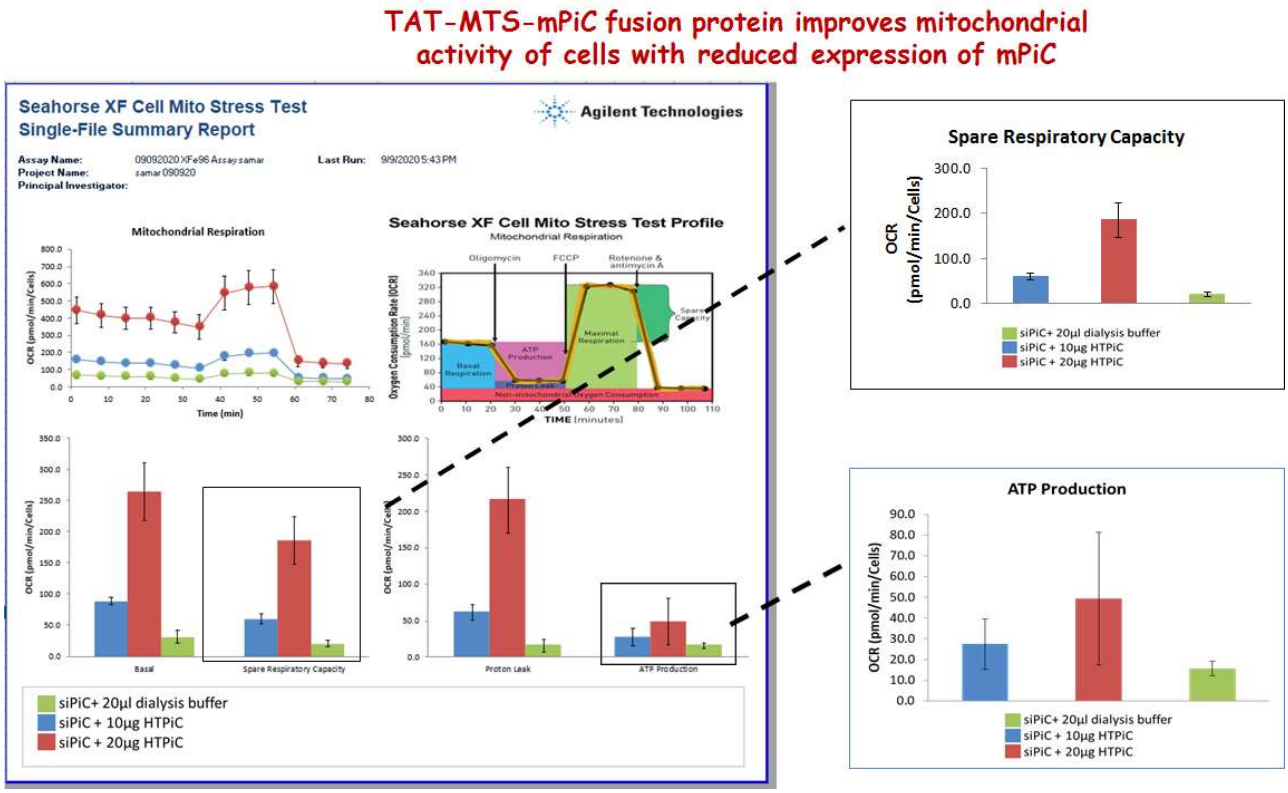

Figure 16. Treatment with TAT-MTS-PiC-A fusion protein improves the mitochondrial bioenergetics of si-mPiC HeLa cells.

TAT-MTS-mPiCA fusion protein improves mitochondrial bioenergetics of cells with decreased expression of mPiC. Hela cells were transfected with esi-mPiCA. After 24 hrs incubation, the media (rich media) was replaced and cells were incubated for an additional 24 hrs. The media was then replaced to poor media without glucose (supplemented with dialyzed FBS, 1% glutamine and 1% p/s). Four hours later TAT-MTS-mPiCA fusion protein was added for an additional 24 hrs, at two concentrations. Mitochondrial function was tested using Seahorse technology.

Additionally, cells with defective oxidative phosphorylation often increase their reliance on glycolysis with conversion of pyruvate to lactate as the main means to regenerate NAD^+. Lactate levels were measured (ABL90 Instrument) in the medium of cells cultured in 25 mM glucose. Lactate levels increased upon PiC-KD by x1.9 fold, then levels decreased to WT levels when PiC-KD cells were treated with TAT-PiC (**Figure 17**).

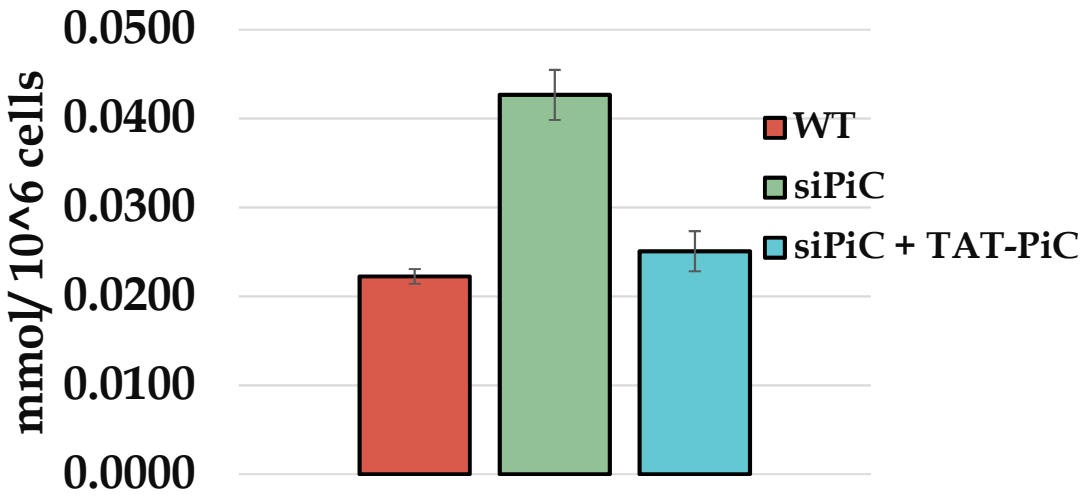

Figure 17: Lactate measured in extracellular medium from wild-type (WT) HeLa cells, Hela cells with transient knockdown of PiC (siPiC), and siPiC cells treated with 30 µg TAT-PiC-A (n=5 independent experiments/cell type)

We further tested the efficacy of TAT-PiC-A to rescue phenotypes in HeLa cells with PiC kd (transient kd by siRNA). To this end, the total cellular phosphate concentration was measured. PiC kd resulted into a substantial decrease in total cellular phosphate (**Figure 18: next page**). Treatment with TAT-PiC-A dose-dependently increased phosphate levels, with the highest concentration P i C resulting phosphate to the level observed in control cells, adding to the list of phenotypes in PiC kd Hela cells that can be rescued by TAT-PiC-A.

Finally, it was reported that the PiC also transports copper (Boulet et al 2018 PMID 29237729). Hela cells were knocked down with siPiC and treated with 30µg TAT-MTS-PiC-A chimeric protein. Copper concentration was determined using the Kit ab272528 (ABCAM). Mitochondrial Cu levels decreased to 75% upon PiC-KD, but were restored, to 119% of control level, in mtPiC-KD cells treated with 30µg TAT-PiC-A (**Figure 19**: **next page**).

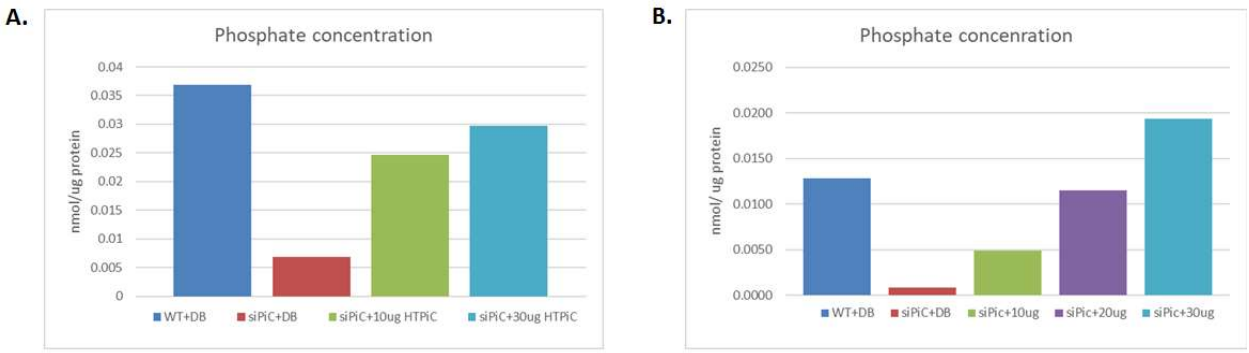

Figure 18: **Phosphate Concentration within Mitochondrial Lysates of Hela Cells deficient in PiC Increases Upon Treatment with TAT-MTS-PiCA Chimeric Proteins**
PiC was depleted from Hela cells using siRNA, then treated with increasing concentrations of TAT-PiC-A chimeric protein. Phosphate concentration were determined using the Kit ab65622 (ABCAM). A&B are two separate experiments performed.

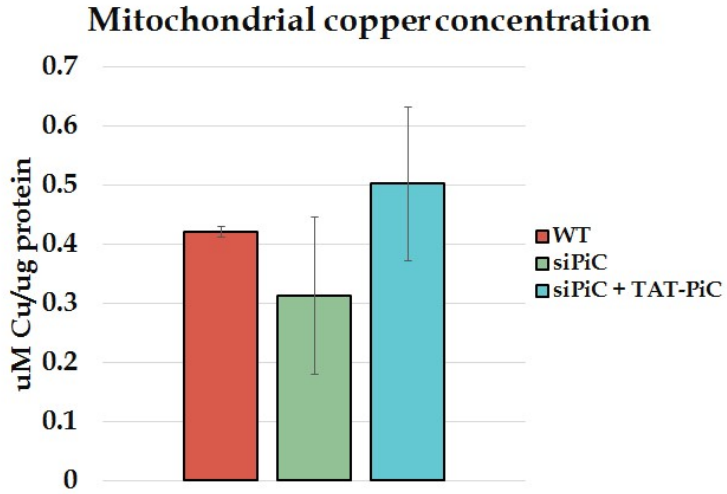

Figure 19: Copper Concentration within Mitochondrial Lysates of Hela Cells deficient in PiC Increases Upon Treatment with 30 µg TAT-MTS-PiC-A Chimeric Protein. 3 independent experiments/cell type.

To summarize the findings:

1) We have purified TAT-MTS-PiC-A and TAT-MTS-PiC-B fusion proteins.

2) We have demonstrated that partially purified TAT-PiC-A is not toxic to cultured cells

3) We have also shown that TAT-PiC-A is internalized into cells, and correctly localizes to the inner mitochondrial membrane.

4) Using transient PiC knockdown (kd) using siRNA in HeLa cells (because we could not generate a knockout cell line by the CRISP/Cas9 technology), we showed that TAT-PiC-A could partially restore the cell proliferation defect that resulted from PiC kd

5) Finally, TAT-PiC-A significantly and dose-dependently improved mitochondrial bioenergetics in HeLa cells with PiC-KD, decreased lactate production, and restored phosphate and copper levels in PiC-KD cells.

4. IMPACT

- **What was the impact on the development of the principal discipline(s) of the project?**

-This project will allow us to understand whether the mitochondrial phosphate carrier (PiC) is absolutely required for the transport of inorganic phosphate into the mitochondrial matrix. Although the latter has in fact been assumed, it was never tested directly because of the lack of adequate models. This project will utilize several new models of PiC depletion to specifically test, for the first time, the requirement of PiC for oxidative phosphorylation (Aim 1) and buffering of Ca^{2+} that enters the mitochondrial matrix (Aim 2). This project will also evaluate how skeletal muscle adapts to PiC which is particularly relevant in the context of mutations in the human gene that encodes PiC that result in myopathies (Aims 1 and 2).

-This project will generate TAT fusion proteins for both PiC isoform (A and B). These may have therapeutic potential for individuals suffering from myopathy caused by variants of the human gene encoding PiC.

- **What was the impact on other disciplines?**

-These studies allow us to evaluate (mal)adaptive mechanisms that arise from mitochondrial dysfunction (due, here, to PiC depletion) and thus to gain broader understanding of cellular and tissue responses to mitochondrial dysfunction. The utility of the latter is 1) to gain a better understanding of basic adaptive mechanisms, and 2) to gain better insight into the pathogenesis of mitochondrial disease which, as is becoming increasingly apparent, is not merely induced by a decline in oxidative phosphorylation.

-Development of TAT-PiC fusion proteins is particularly challenging because PiC is a membrane protein. Development of methods to purify and store TAT-PiC-A in an active conformation might prove useful for the development of other TAT fusion proteins made for membrane proteins.

- **What was the impact on technology transfer?**

  NOTHING TO REPORT

- **What was the impact on society beyond science and technology?**

-This project has provided numerous training opportunities for Masters and Doctoral students as well as post-doctoral fellows, in terms of learning new techniques as well as learning about mitochondrial bioenergetics, cellular Ca^{2+} handling and mitochondrial disease. This project has already benefitted several trainees, namely Dr. Cesar Vasquez (post-doctoral fellow, Seifert lab) who has now had extensive training in the measurements of Ca^{2+} fluxes and in microscopy, and Ms. Samar Zabit (PhD student, Dr. Lorberboum-Galski's lab) in recombinant protein production and purification, and cellular subfractionation. Ji In An from the Seifert lab has also benefitted from participating in this project, by conducting some of the calcium retention capacity

measurements and immunoblots.

5. CHANGES/PROBLEMS

- **Changes in approach and reasons for change**

  No changes in the approach

- **Actual or anticipated problems or delays and actions or plans to resolve them**

  Delays due to Pandemic-related shutdown of labs and forced decrease in mouse colonies has spilled over into delays in publishing.

- **Changes that had a significant impact on expenditures**

  No Changes

- **Significant changes in use or care of human subjects, vertebrate animals, biohazards, and/or select agents**

  Please see the above paragraph addressing significant delays.

- **Significant changes in use or care of human subjects.**

  No Changes

- **Significant changes in use or care of vertebrate animals.**

  No Changes

- **Significant changes in use of biohazards and/or select agent**

  No Changes

6. PRODUCTS, INVENTIONS, PATENT APPLICATIONS, AND/OR LICENSES

- **Publications, conference papers, and presentations**
    - **Journal publications.**

      No. Nothing to Report
    - **Books or other non-periodical, one-time publications.**

      No. Nothing to Report
    - **Other publications, conference papers, and presentations.**

      No. Nothing to Report
- **Website(s) or other Internet site(s)**

  Nothing to Report
- **Technologies or techniques**

  Nothing to Report
- **Inventions, patent applications, and/or licenses**

  Nothing to Report
- **Other Products**

  Regarding “Other products”, we have products in progress, namely the TAT-PiC-A and TAT-PiC-B fusion proteins. However, these proteins remain in the testing phase. Therefore, it does not seem appropriate to report them at this time. Therefore, the answer is: Nothing to Report

7. PARTICIPANTS & OTHER COLLABORATING ORGANIZATIONS

- **What individuals have worked on the project?**

Name:	Erin Seifert
Project Role:	Principal Investigator
Researcher Identifier (e.g. ORCID ID):	0000-0002-8416-5763
Nearest person month worked:	2
Contribution to Project:	Dr. Seifert is the Principal Investigator of this project (Overall decisions about models and studies to be conducted, communication with subawardees and co-investigators, design of Aim 1 studies, direct supervision of Briyanna Hymms contributions to design of Aim 2 studies, coordination of testing of TAT-PiCA protein in cell culture models and design of those studies, responsible for progress reports and quality control of all data and scientific integrity of all studies)
Funding Support:	NA

Name:	Gyorgy Hajnoczky
Project Role:	Co-Investigator
Researcher Identifier (e.g. ORCID ID):	0000-0003-3813-2570
Nearest person month worked:	1
Contribution to Project:	Gyorgy Hajnoczky has performed work in the area of Aim 2 (design of the Ca2+ studies) Dr. Hajnoczky completed his role during this reporting period.
Funding Support:	NA

Name:	Briyanna Hymms
Project Role:	Research Assistant
Researcher Identifier (e.g. ORCID ID):	NA
Nearest person month worked:	4
Contribution to Project:	Briyanna Hymms has performed work in the area of Aim 1 and 2. Her role is to assist Dr Seifert.
Funding Support:	NA

Name:	Noa Hauzer
Project Role:	Student (Hebrew University/Consortium)
Researcher Identifier (e.g. ORCID ID):	NA
Nearest person month worked:	12
Contribution to Project:	Noa Hauzer has performed work by carrying out the planned experiments; including: expression (both two mPiC isoforms-A&B) in bacterial hosts; purification of the fusion proteins (mainly improving and establishment of a purification protocol), testing the proteins on cultured cells regarding its internalization into the cells and into its final destination-the mitochondrial inner membrane; biological activity as phosphate carrier and its effect on cell and mitochondrial function, in cultured cells with reduced endogenous expression (by siPiCm) of the PiC mitochondrial carrier.
Funding Support:	NA

Name:	Samar Zabat
Project Role:	Student (Hebrew University/Consortium)
Researcher Identifier (e.g. ORCID ID):	NA
Nearest person month worked:	12
Contribution to Project:	Samar Zabat has performed work by carrying out the planned experiments; including: expression (both two mPiC isoforms-A&B) in bacterial hosts; purification of the fusion proteins (mainly improving and establishment of a purification protocol), testing the proteins on cultured cells regarding its internalization into the cells and into its final destination-the mitochondrial inner membrane; biological activity as phosphate carrier and its effect on cell and mitochondrial function, in cultured cells with reduced endogenous expression (by siPiCm) of the PiC mitochondrial carrier.
Funding Support:	NA

- **Has there been a change in the active other support of the PD/PI(s) or senior/key personnel since the last reporting period?**

Seifert, Erin
Current Active Research Support:

The below research support has ended:
Title: Molecular Mechanisms of Mitochondrial Ca2+ Transport
Identifier: R01 GM102724
Role: Co-Investigator
Effort: 0 CM
Agency: NIH/NIGMS
Grants Officer/Address: Eileen Hyde, Hydee@nigms.nih.gov
Performance Period: 02/01/15-**02/28/2021**
Level of Funding:

Goal/Specific Aims: 1) to test a mechanistic model for the Ca2+-dependent control of mtCU based on MICU1's interactions with MCU and EMRE and dimerization with MICU1/2/3; 2) to determine the functional and pharmacological relevance of the tissue-specific differences in the molecular composition of the mtCU; 3) to test the role of mitochondrial calcium signaling in mitochondrial metabolism and stress responses of the liver; 4) to determine the MICU1-dependence of neuronal calcium signaling and function.
There is no overlap with the current application.

The below calendar months and project end date has been updated:
Title: Regulation of substrate metabolism in skeletal muscle by mitochondrial thioesterases
Identifier: R01 DK109100
Role: Principal Investigator
Time Commitment: **3.12** CM
Supporting Agency: NIH
Contracting/Grants Officer: Craig Bagdon, bagdonc@niddk.nih.gov
Performance Period: 7/01/17- **6/30/23 * NCE**
Level of Funding:
Project Goals/Specific Aims: The central goal is to determine the biological role and mode of action of the mitochondrial enzyme, Acot2.
There is no overlap with the current application.

The below calendar months and project end date has been updated:
Title: Pathogenesis of Myopathies Caused by Novel Mitochondrial Phosphate Carrier Mutations
Identifier: R01GM123771
Role: Principle Investigator
Effort**: .12 CM**
Agency: NIH
Grants Officer/Address: Vernon Anderson, Ph.D.
Performance Period: 09/01/2017-**08/31/23 * NCE**
Level of Funding:
Goal: To investigate the fundamental role of the PiC in mitochondrial Pi transport, the importance of PiC-mediated Pi transport for oxphos and mitochondrial Ca^{2+} uptake and buffering, as well as the pathogenesis of PiC deficiency in skeletal muscle. These studies will also allow us to delineate the (mal) adaptive mechanisms due to severe mitochondrial dysfunction, which are poorly understood for mutations in nuclear DNA-encoded mitochondrial proteins.
Specific Aims: Aim 1: To test for the role of PiC in skeletal muscle and for critical mechanisms counteracting PiC deficiency. Aim 2: To test whether PiC deficiency causes dysregulation of cytoplasmic and mitochondrial Ca2+, and Ca2+ regulated functions.
Overlap: Currently, Aims1 and 2 of the present DoD application overlap 100% with this R01 application. The NIH NIGMS Program Officer, Vernon Anderson, is aware of this overlap and is willing to revise the Aims of the NIH grant such that there is no longer overlap with Aim 2 of the DoD grant. Additionally, Dr. Anderson has agreed to remove part of Aim 1 of the NIH such that part of Aim 1 of the DoD becomes unique.
Aim 3 of the DoD application has no overlap with the R01 application.

The Below Research support/award is new funding:
Title: Nutrient and Stress Signaling in Frataxin-depleted Heart and Skeletal Muscle
Role: Principle Investigator

Effort: 2.4 CM
Agency: Friedreich Ataxia Research Alliance (FARA) Grants
Officer/Address: Jennifer Farmer
Performance Period: 03/01/2021-02/28/2023 Level of
Funding:
Goal: To determine whether inhibitors of the AMPK and mTORC1 pathways, and the integrated stress responses mitigates skeletal muscle atrophy and cardiomyopathy induced by depletion of Frataxin, a mitochondrial protein required for iron-sulfur cluster biogenesis.
Overlap: No Overlap

Lorberboum-Galski, Haya (Consortium- Hebrew University) Current Research Support

Title: Developing a Novel Treatment Approach for Mitochondrial Diseases Role:
Principal Investigator
Effort: 25%/ 3 calendar months Agency:
Private donation
Grants Officer: Mr. Natan Beilinson
Performance Period: 2018-2022 Level of
Funding:
Goal: Developing a novel approach of organelle-transfer, in this case mitochondrial-transfer: The transfer of whole, healthy normal mitochondria into patients' cells defective in a mitochondrial protein as well as in animal model of a mitochondrial disease
Overlap: None